Provenance and Plio-Pleistocene chronology of sediments in the Okavango Basin

S. Vainer, A. Matmon, Y. Erel, A. J. Hidy, O. Crouvi, M. De Wit, Y. Geller, A. Team

April 8, 2020

Basin Research

Disclaimer

This document was prepared as an account of work sponsored by an agency of the United States government. Neither the United States government nor Lawrence Livermore National Security, LLC, nor any of their employees makes any warranty, expressed or implied, or assumes any legal liability or responsibility for the accuracy, completeness, or usefulness of any information, apparatus, product, or process disclosed, or represents that its use would not infringe privately owned rights. Reference herein to any specific commercial product, process, or service by trade name, trademark, manufacturer, or otherwise does not necessarily constitute or imply its endorsement, recommendation, or favoring by the United States government or Lawrence Livermore National Security, LLC. The views and opinions of authors expressed herein do not necessarily state or reflect those of the United States government or Lawrence Livermore National Security, LLC, and shall not be used for advertising or product endorsement purposes.

Landscape responses to intraplate deformation in the Kalahari constrained by sediment provenance and chronology in the Okavango Basin

Shlomy Vainer[1], Ari Matmon[1], Yigal Erel[1], Alan J. Hidy[2], Onn Crouvi[3], Mike De Wit[4], Yona Geller, ASTER Team[5*]

[1] Institute of Earth Sciences, The Hebrew University of Jerusalem, Jerusalem 91904, Israel

[2] Center for Accelerator Mass Spectrometry, Lawrence Livermore National Laboratory, Livermore, CA, USA

[3] Geological Survey of Israel, 32 Yeshayahu Leibowitz, Jerusalem, 9371234, Israel.

[5] Department of Geology, University of Pretoria, Pretoria, South Africa

[5] CEREGE, Aix Marseille Univ, CNRS, IRD, INRA, Coll France, Aix en Provence, France

[*] ASTER Team: Georges Aumaître, Didier L. Bourlès, Karim Keddadouche

ABSTRACT

The structural depression that occupies the Okavango Basin in southern Africa comprises a depo-centre within the intracratonic Kalahari Basin where sediments of the Cenozoic Kalahari Group have accumulated. The Okavango Basin has been formed due to stretching and subsidence at an area of diffused deformation, southwestwards to the main East African Rift System (EARS). Sediments from two full Kalahari Group sequences, located on opposite sides of the Gumare Fault that forms a major fault within the Okavango Basin, were studied to determine their provenance and chronology. Terrestrial Cosmogenic Nuclide (TCN) 26Al/10Be burial dating was used to constrain a chronostratigraphical framework, and Pb, Sr, and Nd isotopic ratios combined with geochemical and sedimentological analyses were applied to track the source areas of the sediments.Results indicate the following sequence of basin filling: (a) Accumulation between ca. 4–3 Ma during which the currently downthrown (southern) block received a mixture of sediments mostly from the Choma-Kalomo, Ghanzi-Chobe, and Damara terranes, and possibly from the Lufilian Belt and/or Karoo basalts during earlier stages of deposition. Simultaneously, the upthrown (northern) block received sediments from more distant Archean sources in the Zimbabwe and/or Kasai cratons, (b) Hiatus in sedimentation occurred at both sites between ca. 3–2 Ma, (c) Sediments on both sides of the Gumare Fault share a similar source (Angolan Shield) with minor distinct contributions to the downthrown block from the Kasai Craton and local sources input to the upthrown block, and (d) Regional distribution of aeolian sand since at least 1 Ma. The change in source areas is attributed to rearrangements of the drainage systems that were probably linked to vertical crustal movements on the margins of the Okavango Basin. The tectonically induced morphodynamics controlled the landscape evolution of the endorheic basin where vast lakes, wetlands and salt pans have developed through time.

INTRODUCTION

Cratonic sedimentary basins are archives of the hinterland's evolution and provide unique insights into the different stages of basin development, environmental settings, palaeo-geography and associated fluvial networks (Allen & Armitage, 2011; Goudie, 2005; Leighton & Kolata, 1990; Sloss & Speed, 1974). Evolutionary models for cratonic basins usually account for the crustal structure and lithosphere thickness (Heine, Dietmar Müller, Steinberger, & Torsvik, 2008), but do not yet agree on how such basins form (McKenzie & Priestley, 2016). These basins are characterized by the lack of major extensional strain features, such as rifts and crustal or lithospheric thinning (Allen & Allen, 2013; Sleep, 1971), and were suggested to develop mainly due to vertical subsidence of the lithosphere (Daly, Tozer, & Watts, 2019).

The occurrence of the Okavango Basin depo-centre, that is characterized as a passive rift (Yu et al., 2015, 2017), within the elevated intracratonic Kalahari Basin (Figure 1a), is therefore intriguing. The structural trough of the Okavango Basin that is superimposed on the ~750 km width diffused stretched zone of the Makgadikgadi–Okavango–ZambeziBasin (MOZB; McCarthy, 2013; Ringrose et al., 2005) wassuggested to propagate southwestwards from the more discretelydeformed East African Rift System (EARS; Buffordet al., 2012; Fairhead & Girdler, 1969; Huntsman-Mapilaet al., 2009; Kinabo, Hogan, Atekwana, Abdelsalam, &Modisi, 2008; Scholz, Koczynski, & Hutchins, 1976).The basin is situated between elevated structural arches(Gumbricht, McCarthy, & Merry, 2001) overlyingProterozoic and Mesozoic rift structures (Dixey, 1956;Doucouré & de Wit, 2003; Modisi, Atekwana, Kampunzu, &Ngwisanyi, 2000; Reeves & Hutchins, 1982; Smith, 1984).Recent seismic, tomographic, and magnetotellurics studiessuggest that lithospheric stretching is the result of inter-cratonicdifferential tectonic strains of the surrounding Archean cratons (i.e., Congo and Kalahari cratons, Figure 1a; Pastier, Dauteuil, Murray-hudson, & Moreau, 2017; Yu et al., 2017), where the upper mantle is rheologically weak (Moorkamp, Fishwick, Walker, Jones, & Mt, 2019).

The structural framework of the Okavango Basin that is characterized by ongoing neo-tectonic activity (Cooke, 1980; Gumbricht et al., 2001; Haddon, 2005; McCarthy, Green & Franey, 1993; McFarlane & Eckardt, 2007; Shaw, 1985) is well-defined by satellite and aerial imaging (Hutchins, Hutton, Hutton, Jones, & Loenhert, 1976; Mallick, Habgood, & Skinner, 1981; McCarthy, 2013; McFarlane & Eckardt, 2007), and aeromagnetic and gravity surveys (Campbell, Johnson, Bakaya, Kumar, & Nsatsi, 2006; Kinabo et al., 2008; Meier et al., 2014; Modisi et al., 2000; Podgorski et al., 2013). A time frame of formation and evolution of accommodation space, on the other hand, is poorly constrained (Haddon, 2005; Nash & Eckardt, 2016). Temporal development of the main western branch of the EARS and the Kalahari Basin could provide age constrains for the evolution of the Okavango Basin. In the western EARS, subsidence that started during the Miocene was followed by

faulting and formation of rift grabens and volcanism that resumed during the Pliocene and Pleistocene (Ebinger, 1989; Haddon, 2005; Logatchev, Beloussov, & Milanovsky, 1972).

On the margins of the Kalahari Basin, epeirogenic movements occurred during several episodes since the initial Kalahari down-warp, probably in the Late Cretaceous (Haddon & McCarthy, 2005). Following the formation of the African I erosional surface (King & King, 1959), uplift of at least 400 m on the western margins during the late Pliocene occurred (Partridge & Maud, 1987), resulting in the removal of Cenozoic sediments (i.e. Kalahari Group; Haddon, 2005; Stuart-Williams, 1992) and river capturing by the Okavango and Zambezi drainage (Thomas & Shaw, 1991). The erosional scarp of the Kalahari Group along the eastern side of the Okavango Basin was also suggested to result from uplift during the Plio-Pleistocene (du Toit, 1933) or as early as the late Paleogene (Moore, Blenkinsop, & Cotterill, 2009). Calculations of river-morphology forming rates (Derricourt, 1976; Lister, 1979), and biogeographical affinities of aquatic organisms (Cotterill & De Wit, 2011; Day, Bills, & Friel, 2009), suggest that drainage patterns were tectonically rearranged during the Pliocene to early Pleistocene times. This possibly caused the blocking of the southward drainage systems and deposition in the endorheic Okavango Basin (King, 1951; McCarthy, Smith, Ellery, & Gumbricht, 2002). Further uplift on a marginal axis during the Pleistocene resulted in the rejuvenation of several drainages systems while other drainage became dormant (Haddon & McCarthy, 2005).

Time constraints of initial sedimentation in the Kalahari are rare (Matmon et al., 2015). The common wisdom is that deposition started during the Early Cenozoic or Late Mesozoic, as a response to continental-scale subsidence and uplift of surrounding swells (Burke & Gunnell, 2008; Moore & Larkin, 2001). Miocene (or younger) age estimations include poorly age-constrained pollen recovered from fluvio-lacustrine sequences in the Makgadikgadi Basin (Moore, Cotterill, & Eckardt, 2012; Figure 1b) and sedge-like plant fossils from the central Kalahari Basin (Wendorff & Master, 2015). The termination of deposition in the MOZB is constrained by the minimum age of surficial sand that overlay Early and Middle Stone Age artefacts (McFarlane & Segadika, 2001). This sand, that controls the landscape over much of the Kalahari and overlay Middle Stone Age tools also in the southern Kalahari, was suggested to cover the landscape in the early Pliocene (Miller, 2014; Partridge & Maud, 1987). Terrestrial Cosmogenic Nuclide (TCN)-based models confirm an early Pliocene age for the initial sand covering the landscape that was reworked during the Early Pleistocene (Vainer, Ben Dor, & Matmon, 2018a).

Here, we focus on the Plio-Pleistocene spatiotemporal evolution of the Kalahari Group in the Okavango Basin. We measured and modelled TCN concentrations in sediments to provide the first direct dating of sedimentation in the main Kalahari Basin and to constrain depositional phases on both sides of the Gumare Fault, one of the main faults of the Okavango Basin (Figure 1b). Pb, Sr and Nd

isotopic ratios accompanied with major and trace element analyses and sedimentological properties are used to determine the thickness of the Kalahari Group and reconstruct palaeo-drainage patterns. Together, they allow putting the chronostratigraphy of the Okavango Basin in the context of the morphotectonic evolution of the MOZ and Kalahari basins.
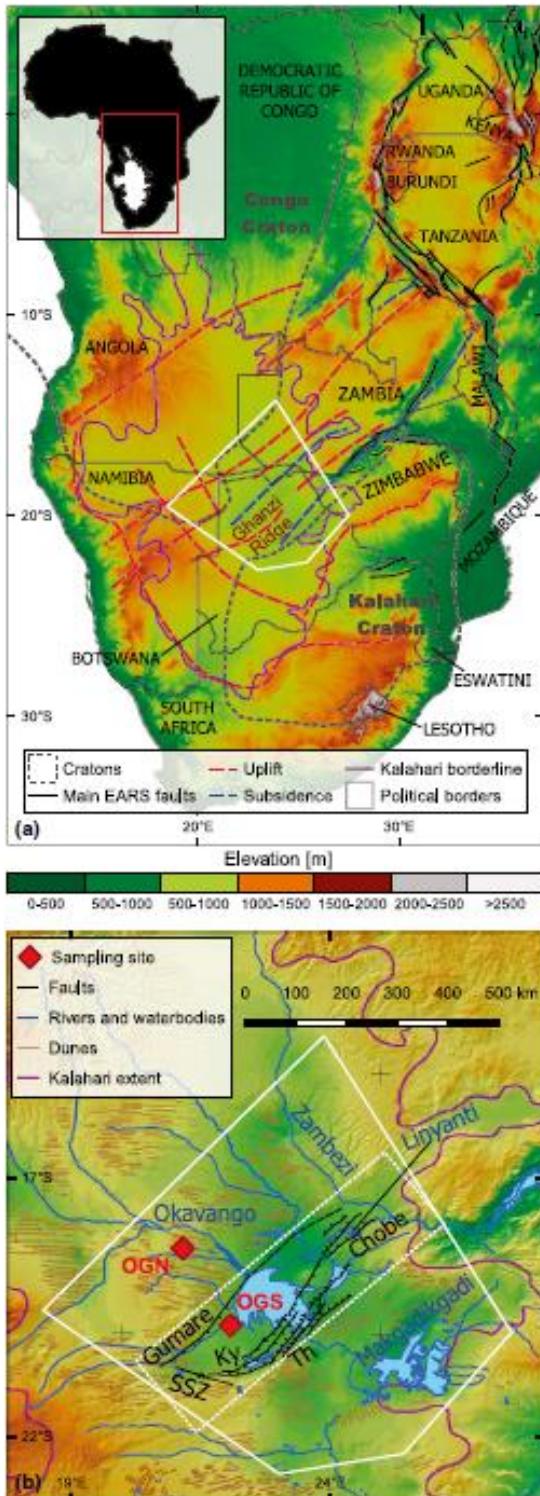
FIGURE 1 (a) Main structural features superimposed on the topography of southern Africa, based on SRTM 30 sec DEM (NASA JPL, 2013). Axes of uplift and subsidence that have been operated since the Neogene are after Haddon & McCarthy (2005). Main faults of the East African Rift System (EAES) that possibly propagate into the MOZB are after Chorowicz (2005). The white polygon marks the Makgadikgadi–Okavango–Zambezi Basin (MOZB) following the definition of Ringrose et al. (2008). The extent the of underlying cratons that bound the MOZB basin are after Pastier et al. (2017) and Yu et al. (2017) where the Kalahari Craton is consists of the agglomerated Kaapvaal and Zimbabwe cratons. Inset: The white area denotes the Kalahari Basin on the African continent. The red rectangle corresponds to the area depicted in this figure. (b) Geomorphology and structure of the MOZB (marked with a white polygon) superimposed on the sub-Kalahari Group (Cenozoic sediments) topography map (from Haddon, 2005), illustrating the accommodation space within the semi-endorheic basin. Location of faults are after Kinabo et al. (2008) and Pastier et al. (2017). Abbreviations of faults are: SSZSekaka Shear Zone; Ky- Kunyere; Th- Thamalakane. Sand dunes are after Thomas & Shaw (1991). Okavango Graben North (OGN) and Okavango Graben South (OGS) indicate the location of the studied boreholes. Dotted rectangle indicates the extent of the Okavango Basin mentioned in the text (excluding headwaters area and including the capturing zone of the Upper and Middle Zambezi)

GEOLOGY AND MORPHOTECTONICS

Structure

The Okavango Basin, located in northern Botswana, is bounded by a series of normal to dextral strike-slip faults (Modisi, 2000; Modisi et al., 2000) forming ~120 km width half-graben at an overall length over 600 km (Figure 1b; Haddon & McCarthy, 2005). The extent of neotectonic subsidence in the Okavango depression has been estimated to be between 300 m (Greenwood & Carruthers, 1973; Modisi, 2000) and 1000 m (Hutchins et al., 1976). Subsidence has outpaced sedimentation resulting in the formation of today's largest inland alluvial fan in Africa (i.e., the Okavango Delta) and the Linyanti wetlands (Figure 1b; Gumbricht et al., 2001; McCarthy & Ellery, 1998). The crustal sagging underneath the delta is thought to be occurring partly as a result of sediment loading (Gumbricht et al., 2001; McCarthy et al., 2002). The main fault that controls the Okavango Delta is the Gumare Fault, having a 20 m high scarp of a dip-slip movement (Kinabo et al., 2008; Modisi et al., 2000). It is considered to form an antithetic fault to the listric Thamalakane and Kunyere faults that bound the Okavango Basin to the southeast (McCarthy, 2013). Upthrow to the southeast of the Thamalakane and Kunyere faults resulted in the formation of the Ghanzi Ridge (Figure 1; Gumbricht et al., 2001) that is suggested to have risen ~100 m since the initiation of the Okavango subsidence (Haddon, 2005). South to the Ghanzi Ridge, the uplifted structure that accommodates the Makgadikgadi depression, where limited hydrological connections with the Okavango exist today, accommodated the world's largest salt-pan complex (Podgorski et al., 2013), but there is evidence for larger hydrological discharges between the two sub-basins in the past, forming big lakes (McFarlane & Eckardt, 2006; Moore & Larkin, 2001). In the northeastern Okavango Basin, the graben structure narrows and is broken into several narrower depressions bounded by north-easterly striking faults, of which the Chobe Fault is the largest. The faults extend to the southwest and terminate against the westerly trending dextral Sekaka Shear Zone (SSZ).

Sediment characteristics and possible sources

Sediment thickness in the Okavango Basin may reach 300 m(Haddon & McCarthy, 2005; Podgorski et al., 2013), but is probably overestimated in places (McFarlane, Eckardt, Ringrose, Coetzee, & Kuhn, 2005). The sediments record phases of lacustrine conditions (Grey & Cooke, 1977; Grove, 1969; McFarlane & Eckardt, 2006; Podgorski et al., 2013; Shaw, 1985; Thomas & Shaw, 1991) that were controlled by climatic variations (Burrough, Thomas, & Bailey, 2009; Cordova, Scott, Chase, & Chevalier, 2017; Lancaster, 1979), and influenced by tectonically induced diversions of drainage systems (Ebert & Hitchcock, 1978; Moore & Larkin, 2001; du Toit, 1933).

Beneath the Kalahari Group, the youngest rocks that occupy the Okavango Basin are siliciclastic sediments of the Karoo Supergroup, deposited in Late Palaeozoic-Early Mesozoic basins (Catuneanu et al., 2005), and mafic lavas and dolerites emplaced during the breakup of Gondwana, mainly between 181 and 179 Ma (Duncan, Hooper, Rehacek, Marsh, & Duncan, 1997; Le Gall et al., 2002). Additional Karoo-age volcanics are widespread over the MOZB's subsurface, mostly towards the east and southeast of the study sites. MOZB basement also includes granites, gabbros, granulites, amphibolites, metarhyolites, metabasalts and siliciclastic and carbonate sedimentary rocks, of various Proterozoic ages that are detailed below (Figure 1a; Kampunzu, Akanyang, Map eo, Modie, & Wendorff, 1998; Kampunzu, Armstrong, Modisi, & Map eo, 1999, 2000; Map eo, Armstrong, & Kampunzu, 2001; Map eo, Kampunzu, & Armstrong, 2000).

Most of the basement rocks in the Kalahari Basin are covered today by sediments of the Kalahari Group. In the past, erosional products of basement rocks could have been transported to the Okavango Basin by rivers sourced within the Kalahari Basin which were suggested to have operated during the Pleistocene (Cooke, 1975). Additional possible sources for detritus filling the Okavango Basin include sediments that have been transported through three main drainage systems. East to west these are the Zambezi, Okavango and several shorter rivers that originate in Namibia (Figure 2). Each of the three main fluvial systems carries sediments that are sourced from several geological domains. Their source rocks, and geochemistry of sediments carried in each drainage system (see methods and data processing section 'provenance analyses') are described below.

Zambezi drainage

The Zambezi system drains two Archean domains. The southern is the granite-greenstone Zimbabwe Craton that formed between 3.55 and 2.58 Ga (Dirks & Jelsma, 2002). The second is the Kasai Craton which lies to the north of the Okavango Basin and includes granulites, amphibolites, granitoids, and gabbros that span over a similar time-range (3.5–2.5 Ga; De Carvalho, Tassinari, Alves, Guimarães, & Simões, 2000; De Waele, & Mapani, 2002; Jelsma, Perritt, Joy, & Armstrong, 2016). An additional contribution to the Zambezi is possible through the drainage of its north-western tributaries, with the Kuando River forming the major channel, sourced at the Angolan Shield (detailed below in 'Okavango drainage'). Also, derivation of sediments is possible through smaller streams sourced close to the MOZB. These streams drain the Proterozoic Choma-Kalomo Block that contains mostly granites and gneisses as well as metasedimentary rocks (Schlüter, 2008; Glynn et al., 2017). Granites of the Choma-Kalomo are Mesoproterozoic in age (1.37–1.18 Ga) while zircons dated in the metasedimentary rocks point to the reworking of Paleoproterozoic crust (2.04–1.86 Ga). Furthermore, this terrane was also suggested to have Zimbabwe-Craton (Archean) origins (Glynn et al., 2017). The Zambezi also drains the copper-bearing volcanics and metasediments of the Neoproterozoic Lufilian Belt (Rainaud,

Master, Armstrong, & Robb, 2005; Thiéblemont, Callec, Fernandez-Alonso, & Chène, 2018). Five sites were chosen to represent the composition of sediments carried by the Zambezi drainage: Tinde, Kasaya and Sinde rivers, and the Victoria Falls and Deka sites at the main Zambezi channel (Figure 2).
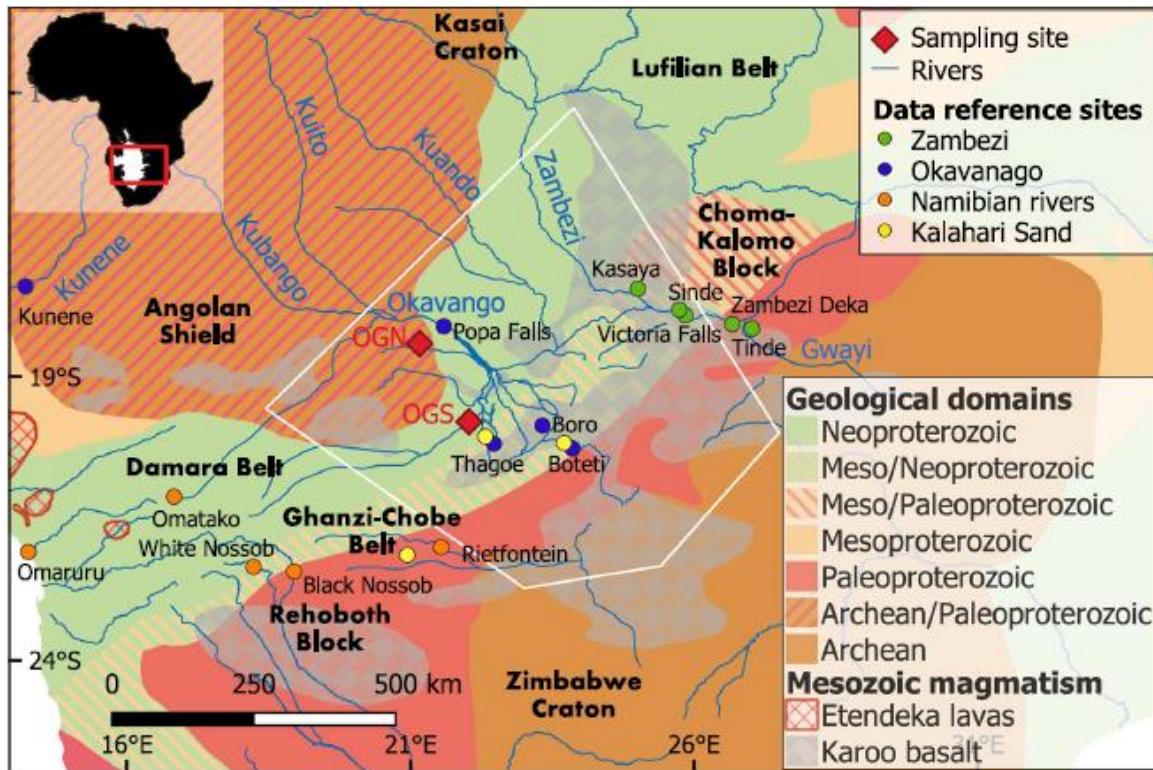
FIGURE 2 Basement geology of the main Kalahari Basin. Geological domains are after Milner, Duncan, Whittingham, & Ewart (1995), Jourdan et al. (2007), Schluter (2008), McCourt et al. (2013), Glynn et al. (2017), and Yu et al. (2007). Data reference sites of current river load are from Garzanti, Padoan, Setti, Lopez-Galindo, and Villa (2014). Okavango Graben North (OGN) and Okavango Graben South (OGS) indicate the location of the studied boreholes. The white polygon marks the Makgadikgadi–Okavango–Zambezi Basin (MOZB) following the definition of Ringrose et al. (2008). Inset: The white area denotes the the Kalahari Basin on the African continent. The red rectangle corresponds to the area depicted in this figure

Okavango drainage

The Kuito and Kubango Rivers, which are the northern tributaries of the Okavango River, drain the Angolan Shield, located on the southern flanks of the Congo Craton. The Angolan shield is also drained by the Kunene River, which flows today to the Atlantic Ocean but was suggested to flow southward during the early Pliocene (Stuart-Williams, 1992). This terrane preserves a history of Neoarchean crustal formation with principal magmatism forming granites, gneisses and volcanics at 2.52 ± 0.1 Ga (Jelsma, Perritt, Armstrong, & Ferreira, 2011), and also composed of Paleoproterozoic orthogneisses, granites, granofels, greenstones, quartzites and schists (De Carvalho et al., 2000; De Waele, & Mapani, 2002; Gartner, Linnemann, & Hofmann, 2014) that formed between 1.97 and 1.76 Ga (Jelsma, McCourt, Perritt, & Armstrong, 2018). Archean and Paleoproterozoic protoliths were intruded during the Early Mesozoic at 1.45 ± 0.05 and 1.33 ± 0.01 Ga (Brandt, Will, & Klemd, 2007). Sediments carried in the Okavango drainage are represented by river load of the Thaoge, Boteti and Boro rivers. Two

additional sites are the Popa Falls on the main Okavango channel and the Kunene River that partially drains similar rocks to those of the main Okavango channel (Figure 2).

Namibian rivers

Northern-most Namibian rivers constitute tributaries of the Kubango and Kunene Rivers that drain the southern outcrops of the Angolan Shield into the Okavango River. More to the south, Namibian rivers pass through the greenschist to granulite metasediments and granitic intrusions of the Pan-African Damara Belt that was amalgamated between 580 and 500 Ma (Gray et al., 2008; Hanson, 2003; Hawkesworth, Menzies, & Van Calsteren, 1986). These rocks constitute the western elevated border of the Okavango Basin. Rivers that currently drain westwards to the Atlantic Ocean also drain Mesozoic volcanics of the Etendeka formation and anorogenic Damara intrusions (Milner et al. 1995). Along the south-western border of the Okavango Basin, older rocks are exposed. The northern terrane among them is the Meso- to Neoproterozoic Ghanzi-Chobe Belt (drained also by the Zambezi and Okavango systems), which is composed of felsic and mafic volcanic rocks that are intercalated and overlain by metasediments that were deposited between ~1.1 and 0.75 Ga (Modie, 1996; Ramokate, Map eo, Corfu, & Kampunzu, 2000; Singletary et al., 2003). The southernmost rocks that could contribute to the sedimentary budget of the MOZB are the volcanoclastics of the enigmatic, Paleoproterozoic to Mesoproterozoic Rehoboth Block (Singletary et al., 2003; Schluter, 2008). Sediments that are carried by Namibian rivers are represented by the following sites: Rietfontein, Omatako, White Nossob, Black Nossob and Omaruru (Figure 2).

METHODS AND DATA PROCESSING

Sedimentology

Two full Kalahari Group sequences were investigated. One from the upthrown block on the northern side of the Gumare Fault (OGN), and one from the downthrown side located on the southern flank of the Gumare Fault (OGS; Figure 1b). Cuttings at one-meter interval reaching to a depth of 117 m at OGN (original name - borehole 9,696) that were drilled during the Northwest Ngamiland TGLP Groundwater Potential Study (Government of Botswana (GoB), 2003a, Government of Botswana (GoB), 2003b) were provided by Margaret Mcfarlane. Similarly, cuttings at one-meter interval reaching a depth of 110 m at OGS, were obtained from the Tsodilo Resources Limited exploration company. Samples were examined using a SMZ800N stereo microscope and selected samples were analysed with a scanning electron microscope (*SEM*; FEI Quanta 200) both for physical properties and chemical composition, at the Hebrew University of Jerusalem, Israel (HUJI). These preliminary analyses were done to select samples for additional, more detailed, analyses. Particle size distribution (PSD) analyses were performed using a Malvern MS-2000 laser diffraction at the Geological Survey of Israel on the <2 mm size fraction after leaching with concentrated HCl and H_2O_2. PSD of 21 samples from OGN and

15 from OGS were analysed. Based on PSD results, each sample was separated into coarse and fine fractions at the minimum value of PSD frequency. Separation occurred at 125 μm for samples from OGS and 63, 75, and 105 μm for samples from OGN (see results and interpretation section 'PSD and mineralogy') with GA-6 GilSonic AutoSiever into fine and coarse fractions (Table S1). For 11 samples from OGS and 10 samples from OGN of both fine and coarse fractions that displayed unique visual characteristics under the microscope, major minerals were determined using X-ray diffractometer (XRD; D8 Advance of Bruker AXS) at HUJI (Table S2).

Cosmogenic nuclides

Concentrations of 10Be and 26Al were measured in quartz separates, purified from the sieved 105–850 μm grain size fraction following standard procedures of HF dissolution and ion-exchange chromatography (Kohl & Nishiizumi, 1992; Bierman & Caffee, 2001) at HUJI. Aluminium concentrations of the dissolved aliquots were in the range of 69–218 ppm, determined using ICP-OES on aliquots at HUJI. 10Be/9Be and 26Al/27Al ratios were measured at two different AMS facilities. Twelve samples were analysed at the European Center for Research and Education of Environmental Geosciences (CEREGE), France, and seven samples were measured at the Lawrence Livermore National Laboratory (LLNL), USA, (Table S3).

Apparent burial ages were estimated by simulating 26Al and 10Be concentrations resulting from TCN build-up during a period of surface exposure followed by radionuclide decay after burial (Granger & Muzikar, 2001). Preburial TCN accumulation was individually estimated for each lithostratigraphical unit over the specifically inferred source area. Specific nuclide production was estimated using the time-varying scaling scheme of Lifton, Sato, and Dunai (2014) yielding 10Be p_0 values between 8.0 and 9.3 atoms g^{-1} yr^{-1}. For sediments buried before 2 Ma, we used the oldest simulated production rates. Post-burial nuclide production by muons was also simulated following Balco (2017), assuming production rates of present-day sample depth and constant sediment bulk density of 2 g cm^{-3} (Hidy, Gosse, Froese, Bond, & Rood, 2013). Probability density functions for individual sample ages with reported 1σ error were calculated via chi-squared inversion of a 2D Monte Carlo simulation that generates 26Al and 10Be concentrations as a function of nuclide build-up and burial durations (Matmon et al., 2015).

Provenance analyses

Elemental and isotopic ratios in sediments have been widely used to reconstruct sediment provenance (e.g., Condie, 1993; Haughton, Todd, & Morton, 1991; Koppel & Saager, 1974; McLennan, Hemming, McDaniel, & Hanson, 1993; Napier, Hendy, Fahnestock, & Bryce, 2020). The combination of Pb, Sr, and Nd isotopes was specifically shown to be useful in discriminating different sources of sediments (Farmer, Barber, & Andrews, 2003; Rodrigo-Gamiz, Martinez-Ruiz, Chiaradia, Jimenez-Espejo, &

Ariztegui, 2015; Vainer, Erel, & Matmon, 2018b). Thus, alongside the determination of the dominant ages of the possible provinces using common-lead isochrone dating, ɛNd and 87Sr/86Sr of separated size fractions of the studied sediments (fine fraction of OGS samples and both fractions of OGN samples) were compared to mud (<32 μm of the bulk mineralogical fraction) that is carried today in each of the three major drainage systems of the MOZB (i.e., Zambezi, Okavango, and Namibian rivers). This dataset, reported by Garzanti et al. (2014), is used to characterize the provinces that possibly contributed sediments to each studied chrono-stratigraphical unit. As diagenetic carbonate is abundant in recent deposits in the Okavango Delta (McCarthy & Ellery, 1998) and in sediments buried within the Okavango Basin (Huntsman-Mapila, Kampunzu, Vink, & Ringrose, 2005), and because the presence of carbonate strongly influences the isotopic ratio of 87Sr/86Sr of sediments (Garcon, Chauvel, France-Lanord, Limonta, & Garzanti, 2014), carbonate was leached out from our samples and is compared only to carbonate-free reference mud samples.

Since different geological domains may overlap in their isotopic fingerprints (Bataille, Laffoon, & Bowen, 2012; Padoan, Garzanti, Harlavan, & Villa, 2011), possible sources of the sediments are also characterized by their geochemical elements. We focus on ratios between elements that are more conservative during weathering and are contrastingly concentrated in felsic and mafic rocks such as Cr/Th, La/Co, and Th/ Sc and rare earth elements (REE; Taylor & McLennan, 1981; McLennan et al., 1993). This is because La and Th are relatively enriched in felsic igneous rocks, whereas Co, Cr, and Sc are enriched in mafic rocks (e.g. Cullers, 2000; Wronkiewicz & Condie, 1987).

REE also have different patterns in felsic versus mafic rocks as they have different affinities while incorporated into magma during differentiation. REE patterns and light REE/heavy REE are represented through chondritic normalized ratios of LaN/SmN, GdN/YbN, LaN/YbN (Taylor & McLennan, 1981), and are compared to REE patterns of sediments in current MOZB rivers (Garzanti et al., 2014). Because Eu and Ce can change their oxidation states while the rest of the REE typically exist in the +III oxidation state, their normalized anomalies concerning their neighbouring REE are also calculated. Ca is often replaced by Eu in the crystallization of plagioclase. Thus, positive/negative Eu anomaly normalized to chondritic values (Eu/Eu . CN, Taylor & McLennan, 1981) usually occurs due to the presence/absence of Ca-rich plagioclase, respectively. Post-Archean Australian shales (PAAS; Taylor & McLennan, 1985) normalized Ce anomaly (Ce/Ce . PAAS) and middle REE positive anomalies (i.e. the ratio between the average of Eu, Gd, Tb, Dy divided by the average of the LREE and HREE, MREE/MREE . PAAS) were shown to accompany the presence of iron oxyhydroxide (Haley, Klinkhammer, & McManus, 2004; Pattan, Pearce, & Mislankar, 2005), thus they also serve to trace weathering products of mafic components (Garzanti et al., 2014).

Isotopic ratios

Pb, Sr and Nd isotopic analyses were performed on a multicollector ICP-MS (NEPTUNE Plus) at HUJI. The dissolved carbonate-free samples were concentrated, separated and purified with appropriate resin for Pb, Sr and Nd, following the procedures described in Erel, Dayan, Rabi, Rudich, and Stein (2006), Stein et al. (1997), and Palchan, Stein, Almogi- Labin, Erel, and Goldstein (2013), respectively. At OGS, isotopic ratios were determined on 14 samples for each isotopic system. Pb isotopes were measured on the coarse fraction samples, while Sr and Nd isotopic ratios were measured on the fine fraction, due to low concentrations of these elements in the coarse fraction. At OGN, because of the heterogeneity in sedimentological characteristics, isotopic ratios were determined on ten samples (twenty sub-samples) for each of the separated grain size fractions. Also, to determine the total thickness of the Kalahari Group sediments at OGN (where the distinction with bedrock is not easily made), all isotopic ratios were also measured on deeper buried samples, until a clear distinction with isotopic fingerprints of the bedrock was made (Figure 3, Table S4).

The measured Pb isotopic ratios of NIST 981 SRM were corrected for the mass discrimination effect by thallium addition. The NIST 981 SRM Pb isotopic analyses of $^{206}Pb/^{204}Pb$, $^{207}Pb/^{204}Pb$, and $^{208}Pb/^{204}Pb$ yielded average values of 16.932 ± 0.03, 15.485 ± 0.03, and 36.670 ± 0.07, (2σ, n = 17), respectively. Sr isotopic ratios were normalised to $^{86}Sr/^{88}Sr$ = 0.1194 to correct for mass fractionation. Multiple analyses of the SRM 987 standard yielded an average $^{87}Sr/^{86}Sr$ value of 0.71028 ± 0.00003 (2σ, n = 15). Nd isotope analyses were normalized to $^{146}Nd/^{144}Nd$ ratio of 0.7219. Analyses of the international JNdi standard yielded an average $^{143}Nd/^{144}Nd$ value of 0.512069 ± 0.00002 (2σ, n = 16). Measured $^{143}Nd/^{144}Nd$ ratios were corrected to a value of JNdi = 0.512115 (Tanaka et al., 2000). The Nd isotopic ratios are expressed as εNd = $[(^{143}Nd/^{144}Nd_{measured}/ ^{143}Nd/^{144}Nd_{CHUR}) - 1] \times 10^4$, where the CHUR value is 0.512638 (Jacobsen & Wasserburg, 1980).

Major and trace elements

The chemical composition of the carbonate-free fraction of the sediment was determined on 50 sub-samples (28 from OGS and 22 from OGN, Tables S5 and S6) that were initially ground into a powder with an agate pestle and mortar. Carbonate was removed by leaching with 0.5 M acetic acid for 24 hr at 50°C while sample tubes were occasionally shaken (Palchan et al., 2013). Residual solids were digested in concentrated HF, HNO3 and HCl acids at 160°C until no visible residue was left. Major and trace element analyses were performed with an Agilent 7500cx ICP-MS at HUJI. Accuracy of elemental analysis was controlled by measuring inter-laboratory standards (T-201, T-207, T-209, G2, BHVO-2, TLM-1) and was <5% for major elements except for Na (<14%), and <10% for trace elements. Silicon

concentration was determined using a Bruker Tracer III-V XRF instrument at HUJI, after calibration with several inter-laboratory standards (G2, BHVO-2, AGV-1, TLM-1, DRN, JGB-1, BIR-1a, JB-1a) and pure quartz. The accuracy for Si was estimated to be <10%. Loss On Ignition values were obtained by measuring the weight loss after heating un-leached powdered samples for two hours at 1100°C.
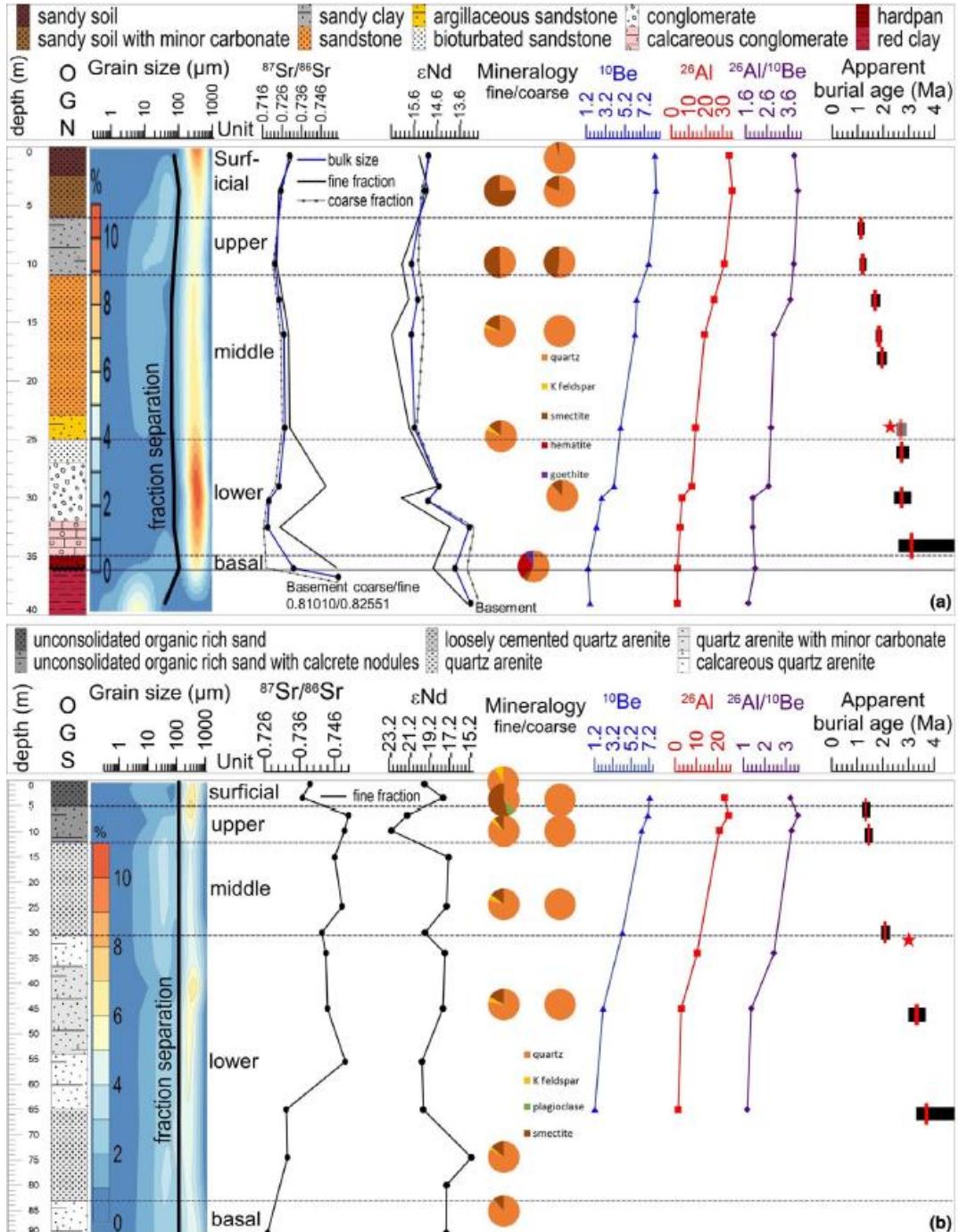
FIGURE 3 Columnar sections of two full Kalahari Group sequences in the Okavango Basin. Data plotted from left to right: Lithology; Carbonate & organic matter-free grain size distribution; Division into lithostratigraphical units that are also separated by horizontal dashed lines. 87Sr/86Sr ratios; εNd values. Symbols are placed where analytical data was obtained; XRD based mineralogy; Cosmogenic nuclides concentrations and ratios; Cosmogenic nuclides-based modeled burial ages. Most probable age is marked red within 1σ range bars. Stars indicate an age that was calculated based on accumulation rates of neighbouring strata from the same unit. (a) OGN site. (b) OGS site

RESULTS AND INTERPRETATION

Chrono-stratigraphical units

By combining all results listed below, we delineate the thickness of the Kalahari Group to 90 m for the sedimentary sequence at OGS (easily distinguished from the underlying amphibolite), and 36 m thickness at OGN where a clear distinction exists between isotopic ratios of Kalahari Group sediments and the underlying bedrock (Figure 3a). The thickness agrees with the isopach of Haddon and McCarthy (2005). The nearly threefold difference in the sedimentary thickness implies ongoing subsidence of the downthrown block, where OGS is located.

We combined the sedimentological and chronological properties (i.e. lithology, PSD, mineralogy, and apparent burial age) to divide each section into subunits according to their chrono-stratigraphical characterization: basal, lower, middle, upper and surficial units (Figure 3). The variations between samples within each subunit are quantified in Table S7. At OGS, units are defined as follows: Basal (90–83 m), lower (82–31 m), middle (30–12 m), upper (11–6 m), surficial (5–0 m). At OGN, where lithological differences throughout the profile are more pronounced than at OGS, the hardpan sample from 36 to 35 m depths defines the basal unit. Samples between 34 and 25 m depths comprise the lower conglomerate-dominated unit. The sandstone between 24 and 12 m depths specifies the middle unit. The upper unit is composed of sandy clay between 11 and 6 m depths. Finally, the upper 6 m that are composed of sandy soil are labelled as the surficial unit.

PSD and mineralogy

Sedimentological variations exist between units that were deposited at the same time at both sites. The basal and lower units at OGS show similar PSD (Figure 3b). They are both composed of 50%–65% fine detritus (except the sample at 40 m depth with 40% fine detritus). Both units are quartz-rich with over 75% quartz in the fine fractions and nearly pure quartz arenite in the coarse fraction. The basal and lower units at OGN are more heterogeneous (Figure 3). The basal unit at OGN is composed of c. 40% fine material of which nearly 40% are iron oxide grains, precipitated by iron-rich solutions. The iron oxides precipitate forms an HCl-resistant cement for the lower unit that is composed of >75% coarse grains. Middle units differ from the units below, but they show a higher similarity between sites, mostly in the fine fraction (Table S7). These units have the highest proportions of fine material relative to the other units in each site (except the basal unit at OGN), but while this fraction constitutes > 59% at OGS, it ranges between 28% and 38% at OGN. Also, both middle units contain mostly quartz and similar proportions of smectite and K feldspar.

The upper and surficial units of OGS are composed of finer material than the equivalent units at OGN. At OGS, PSD mode increases from 204 μm in the upper unit to 235 μm in the surficial unit (mean PSD values increase from 158 to 168 μm). At OGN, PSD mode increases from 316 to 353 μm for the upper and surficial units, respectively (mean PSD value changes from 230 to 349 μm). The

variations between upper and surficial units in each site are attributed to the higher proportion of clay minerals in the upper units (Figure 3, Table S2). Due to the overall PSD similarity at OGS, the separation between fine and coarse fractions for all OGS samples was performed at the minimum of PSD frequency of 125 µm. Because PSD throughout OGN is more variable, the separation between coarse and fine fraction at OGN was done separately for each sample, at 63, 75 and 105 µm (Figure 3, Table S1).

Cosmogenic nuclide

Of 19 samples that were analysed, 17 measurements of both $^{10}Be/^9Be$ and $^{26}Al/^{27}Al$ were significantly distinguishable from blank values (Table S3). Isotopic concentrations below 70 m at OGS and 36 m depth at OGN were too low to yield meaningful burial ages. The resulting ^{10}Be and ^{26}Al concentrations range between $1.22 \pm 0.04 \times 10^5$ and $8.92 \pm 0.24 \times 10^5$ atoms g^{-1} quartz and 1.30 ± 0.22 and $34.13 \pm 1.74 \times 10^5$ atoms g^{-1} quartz, respectively, and $^{26}Al/^{10}Be$ ratios between 1.18 and 4.05. At both sites, ^{10}Be and ^{26}Al concentrations generally decrease down-sequences (Figure 3) implying an undisturbed profile after sediment deposition (Brown, Colin,& Bourles, 2003).

^{26}Al and ^{10}Be concentrations were used to calculate burial ages by applying the approach of Hidy et al. (2013). This approach assumes the present mass-depth of the sample over the entire time of burial. We argue that during the time of burial, periods of thinner overburden, at which production of cosmogenic nuclides by muons was enhanced, were very short compared to the total time of burial (e.g. during the time of sediment accumulation). Periods of thicker overburden, at which production of cosmogenic nuclides by muons was reduced, could have been quite long. Thus, when no other indications are available, the present depth provides a maximum depth of burial.

Major and trace element composition

Elemental concentrations were normalized to Upper Continental Crust (UCC) values to emphasize specific depletions or enrichments of elements, between the sites and between units in each site (Figure 4). At both sites and for both size fractions, weathering is expressed in depletions relative to UCC of Na, K, Ca, Rb, and Sr while Si is enriched in all samples. Different sources and/or different depositional environments between sites are deduced from variations of average elemental concentrations between equivalent chronostratigraphical units (Table S7). Within each site, variations between fine and coarse grainsize fractions are reflected both in mobile and immobile element composition, implying different sedimentological processes for each fraction. Fine fractions at both sites are enriched in REE and all major elements (Figures 4 and 5). The only exceptions are Si that is enriched in the coarse fraction, and Mg that is enriched in the basal sample at OGS and the middle unit at OGN.

Coarse fraction samples from OGS are composed of quartz (Table S2) and have lower concentrations of all elements at all depths in comparison to coarse samples from OGN. The only exception exists between the surficial units, where OGS samples have a slightly higher abundance of Mg, Na, K, Ca, Rb, Sr, Zr, Ba and U.

Fine fraction samples of the middle unit display the highest similarity between sites (Table S7), especially in the abundance of period 4 transition metals (i.e. Ti, Fe, Mn, Sc, Cr, Co, Ni). The lower-most samples of these units at both sites have unique characteristics. At OGS, the sample from 30 m depth has the second-highest content of MgO and Al2O3 (only the abnormal sample from 55 m depth has higher values, see below results and interpretation section for 'Pb, Sr, and Nd isotopic ratios') that may suggest high clay content. At OGN, the coarse sample from 24 m depth has the highest TiO2 and Zr content relative to all other coarse samples. The enrichment of these elements could result from releasing more labile elements during long transportation, or due to in-situ accumulation resulting from intense weathering (Fitzpatrick & Chittleborough, 2002).
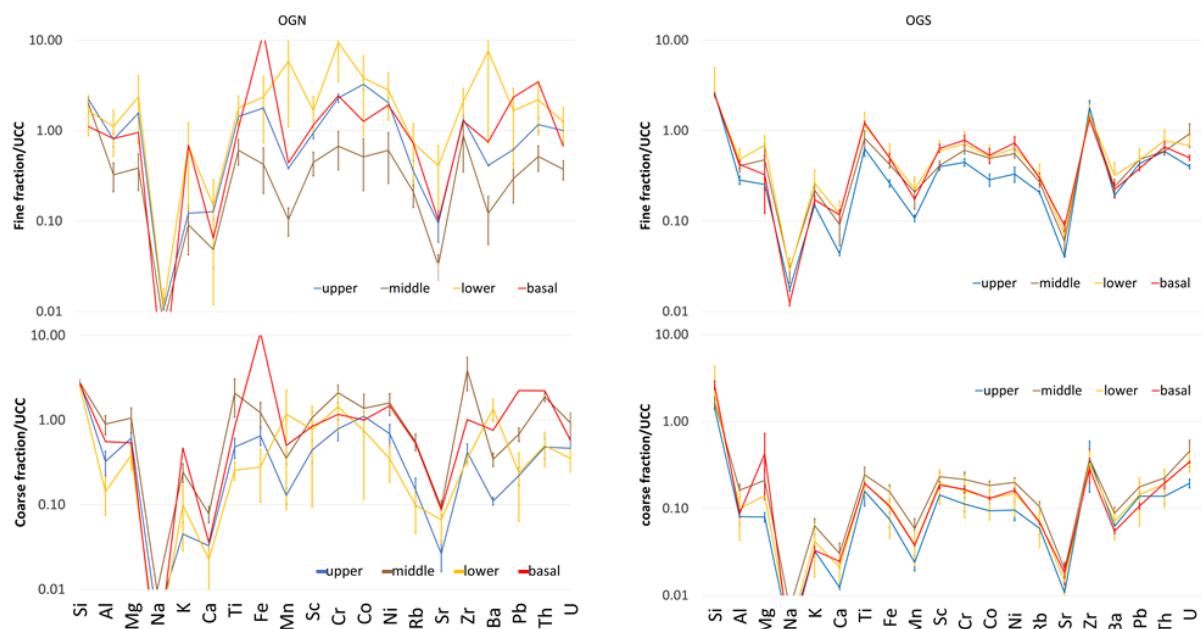
FIGURE 4 Upper continental crust (UCC, Taylor and McLennan, 1985)-normalized elemental abundance of Kalahari Group at OGN and OGS study sites in the Okavango Basin. Curves in each plot are the average values of four chrono stratigraphical units in each section (i.e. basal, lower, middle, upper) and error bars are the standard deviation of each unit. Surficial samples data are omitted to ease the visualization for the rest of the strata

Pb, Sr, and Nd isotopic ratios

Lead isotopic ratios were used to construct regression lines in the 207Pb/204Pb versus 206Pb/204Pb system. The slope of the line in the common lead system can be interpreted as the crystallization age of the source rocks of the sediment (Faure, 1997), or an average age or several terranes when multiple sources are considered. Two apparent isochrons were constructed from coarse fraction samples of

two lithological units in each of the sites where each regression line is composed of four samples (Figure 6). Where high similarity in geochemical and sedimentological proxies exists between samples from neighbouring units from the same site, units were combined to increase the number of samples to yield a more reliable model age.
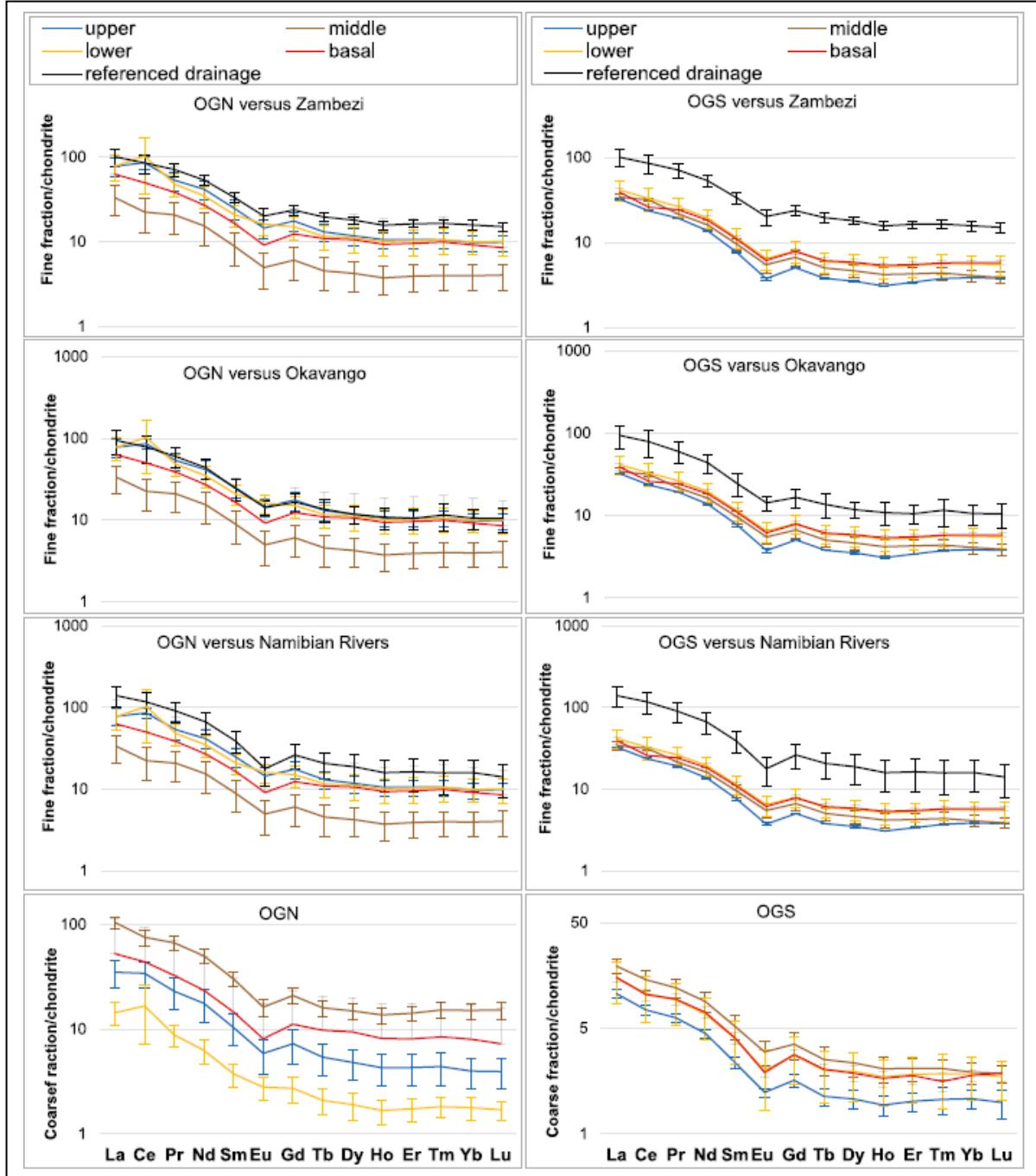
FIGURE 5 Chondrite normalized REE patterns of Kalahari Group at OGN and OGS study sites in the Okavango Basin. Curves in each plot are the average values of four chrono-stratigraphical units in each section (i.e. basal, lower, middle, upper) and error bars are the standard deviation of each unit. Surficial samples data are omitted to ease the visualization of the rest of the strata. Mud fraction average data (<32 μm, Garzanti et al., 2014) of modern rivers are plotted in black lines for comparison with the fine sedimentological fraction of the studied sediments. Error bars are the standard deviation of each drainage system (n=5)

The lower unit at OGS contains sediments derived from a source rock with a model age of 1,128 ± 70 Ma (1σ, MSWD = 13). The sample from 55 m depth, which also has the most radiogenic Sr and Nd isotopic ratios among the lower unit (Figure 3b) and exceptionally high concentrations of all measured period 4 transition metals (Figure 4, Tables S5 and S6), was excluded from the model age calculation due to overdispersion. The relatively similar (RSD = 5%, Table S7) middle and upper units at OGS were combined to yield an age of 3,059 ± 33 Ma (1σ, MSWD = 7.3). An outlier sample from 15 m depth was excluded from the model age calculation.

At OGN, all analysed samples of the basal and lower units display an apparent Pb model age of 3270 ± 125 Ma (1σ, MSWD = 7.8), while samples of the middle and upper units yield a model age of 1928 ± 225 (1σ, MSWD = 2.5).

87Sr/86Sr values of the fine fraction of OGS samples range between 0.72684 and 0.74904 (average 0.741). This 87Sr/86Sr range is similar to the fine fraction of OGN samples (0.72344 to 0.75565), but OGN values are generally less radiogenic than OGS (average 0.728). The coarse sedimentary fraction at OGN has a narrower and lower range of 87Sr/86Sr than the fine fraction, between 0.71654 and 0.72949 (average 0.723).

εNd values of the fine fraction range between −23.0 and −17.3 (average −19.0) at OGS and between −16.6 and −13.9 (average −15.4) at OGN. The coarse fraction at OGN has εNd values between −15.5 and −12.9 (average −14.7). Thus, both Sr and εNd fingerprints suggest more felsic components at OGS (Figure 7).

Throughout the OGS sequence, 87Sr/86Sr ratios remain relatively constant for the lower, middle and upper units, except for the bottom-most analysed sample of the lower unit (at 65 m depth). The basal and surficial units at this site, display less radiogenic values. εNd profile at OGS displays a similar pattern, except from the sample of 10 m depth, which is the least radiogenic throughout the section (Figure 3b).

At OGN, where isotopic ratios were determined separately on the different grain size fractions, 87Sr/86Sr and εNd values and patterns are similar for both fractions at all units with higher variability for the basal and lower units (Figure 3a). Samples of the fine fraction of the middle and upper units at OGN yielded an apparent isochron in the Rb-Sr system, that is more sensitive than Pb-Pb model ages to later magmatic or metamorphic events (Black & Shaw, 1995). The regression line points to magmatism of Karoo age (187 ± 20 Ma, 1σ, MSWD = 5.5, Figure 8).
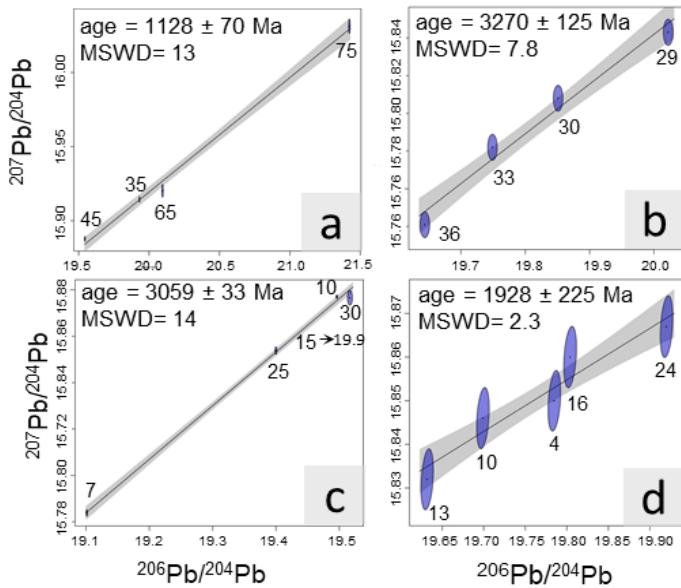
FIGURE 6 Common-lead apparent isochrons and model ages constructed from four different chronostratigraphical units, two in each study site. The depth of each sample is indicated next to its isotopic value. (a) lower unit at OGS. (b) lower unit at OGN. (c) middle and upper unit at OGS, excluding an outlier sample from 15 m depth. (d) middle and upper units at OGN. Plots, age, and 1σ error calculations were done by IsoplotR (Vermeesch, 2018)
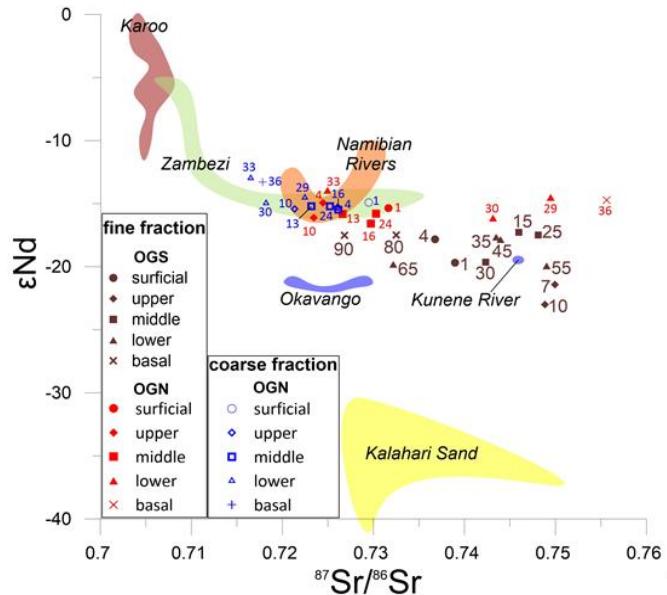
FIGURE 7 εNd versus 87Sr/86Sr of Kalahari Group at OGN and OGS study sites in the Okavango Basin. Numbers indicate the depth of each sample. Colored fields represent the range of isotopic values that were reported from possible sources for the sediments in our study sites. These are: 1. mud samples that were collected in modern rivers, and the aeolian Kalahari Sand samples that were collected from sand dunes (Garzanti et al., 2014); 2. Rocks formed during the Jurassic volcanism (i.e. Karoo province, Jourdan et al., 2007)
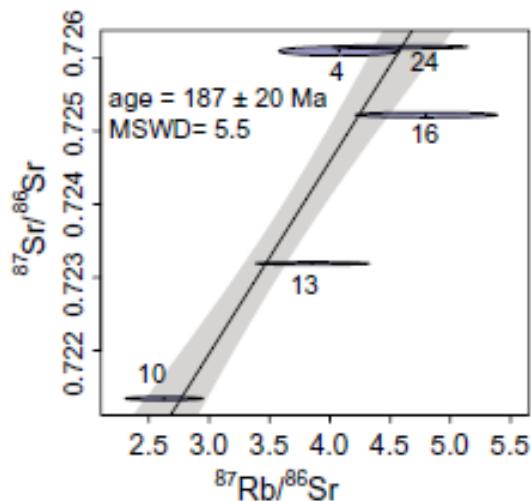
FIGURE 8 Rubidium-strontium apparent isochrone that was constructed from the fine fraction of middle and upper units at OGN. Plot, age, and 1σ error calculations were done by IsoplotR (Vermeesch, 2018)

18

DISCUSSION

It has been argued that geomorphological features in the Okavanago and MOZ basins have experienced recent neotectonic activity that is recorded in the surficial sand around the Gumare Fault (Eckardt, Flugel, Cotterill, Rowe, & McFarlane, 2016; McFarlane & Eckardt, 2007). Here, we focus mostly on the older, Plio-Pleistocene geomorphic evolution of these basins. We combine TCN burial dating with chemical and isotopic analyses to follow the temporal changes of the sediment sources to the Okavango Basin while comparing contemporaneous contributions at the upthrown (OGN site) and downthrown (OGS site) blocks of the Gumare Fault.

Basal and lower units
Chronostratigraphy

The 3.75 +1.34/−0.41 Ma burial age, obtained from 66 m depth at OGS, marks the earliest directly dated deposition of the Kalahari Group. This depositional phase continued at least until 3.35 +0.39/-0.26 Ma during which 20 m of sediments were accumulated (Figure 3b). Assuming similar accumulation rates for the remaining top 15 m of the lower unit at OGS (1 m 20 Ka−1, n = 2), this phase ended around 3 Ma. The lower unit at OGN was deposited shortly after, between 3.06 +4.4/−0.46 and 2.73 +0.22/−0.19, n = 3) allowing erosion of pre-existed strata to occur (McFarlane, Coetzee, Kuhn, Vanderpost, & Eckardt, 2007). This may suggest that differential structural geometry already existed during the Pliocene.

The inability to determine burial ages of the basal units from both sites due to low concentrations of both TCN leaves some uncertainty concerning the earliest deposition of the Kalahari Group in the western Okavango Basin. Low concentrations also suggest that if any exposure of the basal units occurred, it was short such that no significant accumulation of TCN occurred. Because we use present-day topography for modelling pre-burial production while Pliocene topography in source areas was probably lower (see section 'upper and surficial units'), we possibly overestimated production during build-up, which will indicate that the evoked ages represent a maximum time of burial. Nonetheless, modelling end-member production rates reveal that the yielded age has low sensitivity to this parameter, which is within the 2σ range. Although low TCN concentrations could be the result of a long period of burial and the decay of the measurable TCN inventory, relatively low pre-burial concentrations are plausible since early basin fills are often derived from rapidly eroding landscape (Cockburn, Brown, Summerfield, & Seidl, 2000) such that initial sedimentation probably occurred during the early Pliocene.

Sediment sources

During the deposition of the basal and lower units in the two studied sites, sediments were transported from different source areas (Figure 9). Mesoproterozoic granitoids and gneisses of the

Choma-Kalomo block (de Waele et al., 2000, 2002; Eglington & Armstrong, 2002; Glynn et al., 2017), as well as ~1 Ga old marginal granites of the Damara Belt (Key & Rundle, 1981; Hanson, 2003) constitute the main sedimentological assemblage of these units at OGS. Mafic components from the Lufilian Belt of mostly Neoporotozoic age (Rainaud et al., 2012; Thiéblemont et al., 2018) and/or Mesozoic Karoo basalts (Duncan et al., 1997) could have also contributed sediments, during early sedimentation. This is based on the following lines of evidence.
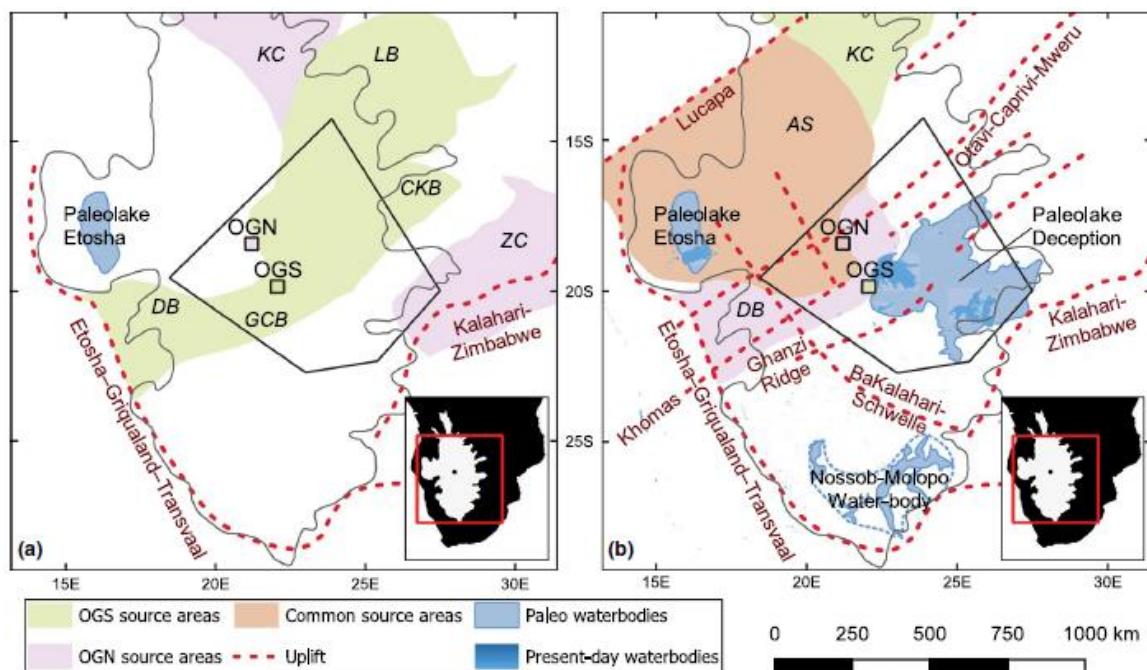
FIGURE 9 Proposed reconstruction of capture areas for the western Okavango Basin during the Pliocene (a) and the early Pleistocene (b), including the extent of current waterbodies. Possible source areas for each of the studied sites (OGN & OGS) were assessed based on characteristics of the buried sediments including their Particle Size Distribution, mineralogy, Pb, Sr, and Nd isotopic ratios, and elemental composition. Abbreviations of the probable terranes that served as sources for the sediments are: DB- Damara Belt; GCB- Ghanzi Chobe Belt; CKB- Choma Koloma Block; LB- Lufilian Belt; ZC- Zimbabwe Craton; KC- Kasai Craton; AS- Angolan Shield. The change in provenance is attributed to adjustments of the drainage systems to crustal uplift along the Otavi-Caprivi-Mweru, and possibly the Lupaca axes (structural axes are after Haddon & McCarthy, 2005). Similarly to uplift along the Etosha-Griqualand-Transvaal axis that triggered the accumulation of Paleolake Etosha (Stuart-Williams, 1992) and the Nossob-Molopo waterbody (Vainer et al., 2018b), an axial uplift along the Kalahari-Zimbabwe and the Ghanzi Ridge probably resulted in the formation of Paleolake Deception and the Okavango Delta (Moore et al., 2012). The inner polygon in each figure marks the Makgadikgadi–Okavango–Zambezi Basin (MOZB) following the definition of Ringrose et al. (2008) and the external outline denotes the extent of the Kalahari Basin as defined by Haddon & McCarthy (2005). Inset: The white area denotes the Kalahari Basin on the African continent. The red rectangle corresponds to the area depicted in the figures

1. The 1128 ± 70 Ma common-lead model age that was yielded from the coarse fraction of the lower unit (Figure 6a) overlaps with crystallization ages of the mentioned provinces (except the karoo). The notable overdispersion of the data (MSWD = 13) is possibly due to scattered ages (Vermeesch, 2018), thus the isochrone could point on the mixing of several terranes with a late Mesoproterozoic average age.

2. The coupled ϵNd versus 87Sr/86Sr fingerprints of the basal and lower units do not match those of the sediments in the referenced drainages but allow mixing between the mentioned adjacent

20

provinces, as the isotopic values lie in between the fields of the rivers that drain these terranes (i.e. Okavango/Kunene, Zambezi, and Namibian rivers, Figures 2 and 7).

3. The relatively wide range in 87Sr/86Sr ratios (Figures 3b and 7) further suggests the incorporation of several sources. While the more radiogenic 87Sr/86Sr ratios may have been derived from the closely outcropping (<100 km) granites that are characterized by 87Sr/86Sr values of over 0.8 (Key & Rundle, 1981), the lower 87Sr/86Sr values of the basal samples (where an isochron age was not determined so we cannot establish a source rock-age connection) may represent some contribution of mafic lithologies, that are more widespread in the Lufilian Belt (Thieblemont et al., 2018) and also in the Mesozoic Karoo rocks (Le Gall et al., 2002).

4. The fine fraction of the basal unit shows a slightly better resemblance of elemental ratios to mafic sources (although still mostly felsic) than the lower unit (Table S7). Accompanied with the similarity of REE ratios between the basal unit and Zambezi-type sediments (Figure 5, Table S7), these characteristics support the suggested westward orientation of the ancient Zambezi tributaries (Shaw & Thomas, 1988), that drain ample amounts of the Lufilian Belt and the Karoo basalts in the present (Figure 2).

The equivalent units at OGN originated from more distant sources than the sediments at OGS and display less variability in source-areas but vary lithologically between the two size fractions (Table S7). The basal and lower units at OGN are dominated by mafic sediments that were derived from the Archean Zimbabwe and/or Kasai cratons. While Paleoarchean and Mesoarchean magmatism are not common in the southern parts of the Archean Congo Craton (i.e., Angolan Shield, McCourt, Armstrong, Jelsma, & Mapeo, 2013), the 3270 ± 125 Ma common-lead model age of the coarse samples of these units (Figure 6b) coincides with early crystallization of the Zimbabwe and Kasai cratons (Dirks & Jelsma, 2002; Jelsma et al., 1996; Thieblemont et al., 2018). Moreover, єNd versus 87Sr/86Sr signature of the Zambezi River (that drains the Zimbabwe and Kasai cratons) are similar to the values of both fractions of the basal unit and the coarse fraction of the lower unit at OGN (Figure 7).

The fine fraction samples of the lower unit at OGN have more radiogenic 87Sr/86Sr ratios than the coarse samples (Figures 3a and 7). These fine fraction samples also have the lowest Th/Cr ratios throughout the sequence, where the second-lowest values are found in the coarse fraction of the same unit (Table S7). Samples of both fractions have Th/Cr ratios that characterize mafic source rocks (Cullers, 2000). Moreover, samples of the lower unit do not have pronounced negative Eu anomaly as the lower unit at OGS and have positive Ce anomaly like in some of the modern MOZB-drained river load (although to a lesser extent, Figure 5). Such REE pattern may represent the weathering products of altered basalt (Bea, 2015; Marsh, 1991), but can also be the result of sedimentological sorting

(McLennan et al., 1993) or in-situ chemical weathering that should increase the Ce/Ce* anomaly (Braun et al., 1990).

Although mafic rocks usually have low 87Sr/86Sr values because of low Rb concentrations, tholeiitic mafic rocks of the northwestern Zimbabwe Carton, as well as the rocks of the gabbro-noritic complex at the southern Kasai Craton, have unusually high 87Sr/86Sr values of more than 0.9 (Delhal, Ledent, & Torquato, 1977; Jahn & Condie, 1976). Hence, these Iron-rich rocks can account for the 87Sr/86Sr values and εNd values of the basal and lower units at OGN (Baldock & Evans, 1988; Delhal, Deutsch, & Denoiseux, 1986), and could supply dissolved Fe(II) for the iron oxides that cemented them. Based on our data, neither of these terranes can be ruled out and different studies suggest both cratons as possible source rocks. The lack of west-bank tributaries in the Gwayi River (Figure 2) and the nature of fluvial deposits in NW Zimbabwe that were suggested to result from original westwards flow of streams towards the Okavango Basin (Shaw & Thomas, 1988), support the Zimbabwe Craton being the main source for sediments that were deposited during the Pliocene at OGN. Two additional observations support the Kasai Craton being the more probable source: (a) Geochemical provenance study showing that deeply buried sediments beneath the Okavango Delta were partially derived from Angola (Huntsman-Map ila et al., 2005) where the Kasai Craton is exposed (b) The southerly drainage system that operated throughout the Kalahari at the same time (Vainer, Erel, et al., 2018) could have delivered sediments from the Kasai Craton that is located to the north of the site.

Middle unit
Chronostratigraphy
The accumulation phase of the middle unit that started around 2 Ma and followed a hiatus of several hundreds of thousands of years (Figure 3; Table S3), instigated by either prolonged or massive erosion. The sample that marks the resumed deposition at OGS (30 m depth) yielded a burial age of 2.04 +0.19/-0.16. The high clay content that is inferred for this sample (see results and interpretation section 'major and trace element composition') could result from a period of surface exposure, that would increase the 26Al/10Be ratio, yielding a minimum apparent burial age. These Mg-rich clays could have also been carried to the site by fluvial systems or precipitated in situ at 3–4 m depth groundwater environment (McCarthy et al., 1993; McCarthy, McIver, & Verhagen, 1991; Ringrose et al., 2008). These scenarios do not support a period of long exposure thus they would imply that the yielded age reasonably represents the time of deposition. This can be supported by the high resemblance of PSD with the rest of the unit above (Table S1), suggesting that sediment of the middle unit went through similar transportation processes and that later alteration by groundwater occurred resulting in clay formation. The yielded age is also confirmed by two of the three dated samples in the equivalent unit at OGN that yielded burial ages within the same range of 1.83 +0.14/0.15 and 1.69

+0.14/-0.14. The third, deepest sample from 24 m depth yielded a burial age of 2.69 +0.19/−0.18 Ma which does not correspond to the ages of the rest of the unit. However, this sample has characteristics that suggest a long transportation time (see results and interpretation section 'major and trace element composition'). Such a process, with possible intermediate deep storage in en route sites, will result in an older apparent burial age. Assuming the same average accumulation rates as the sediment above (1 m 50 Ka−1, *n* = 3), the sample that marks the renewed deposition at OGN was buried at 2.25 +0.20/−0.17 Ma, which is the same apparent age (within error) as the bottom-most sample of the middle unit at OGS.

Sediment sources

The sediments of the middle unit at OGS were probably derived from the Paleoproterozoic components of the Angolan Shield (McCourt et al., 2013) and the Paleoarchean rocks of the Kasai Craton (Jelsma et al., 2018; Figure 9). This is based on both the Mesoarchean Pb-Pb model age (Figure 6c) that could result of mixing between these terranes, and the εNd versus 87Sr/86Sr plot (Figure 7), where samples lie either close to Kunene River values (draining the Angolan Shield) or in between Kunene River and Namibian rivers (draining also the Angolan Shield) and Zambezi values (draining the Kasai Craton, Figure 2). There is also an indication based on the elemental ratios of Th/Cr and La/Co alongside Eu/Eu* and MREE/MREE* values that the coarse fraction of the middle unit at OGS received sediments from a new source that was not present in the lower unit. These geochemical fingerprints point towards more mafic components relative to the units below (Table S7), possibly due to the incorporation of iron-rich, Kasai Craton-sourced weathering products. Also, REE ratios of the coarse fraction do not show an indicative resemblance to any of the referenced drainage systems, suggesting mixing of sources. REE ratios of the fine fraction differ from those of the coarse fraction, resembling ratios of sediments carried by Namibian rivers (Table S7) that probably contribute a higher proportion of fine detritus.

At OGN, the sediments of the middle unit were probably derived from the Angolan Shield and the Damara Belt (Figure 9). This is based on their Paleoproterozoic Pb-Pb model age of 1928 ± 225 (Figure 6d) that could be the result of mixed sediments derived from these terranes, as such mixing would result in an apparent corresponding age (Hanson, 2003; Jelsma et al., 2018). Both provinces are drained by north Namibian rivers (Figure 2) that overlap with most of the samples on the εNd versus 87Sr/86Sr plot (Figure 7). Elemental ratios of Th/Cr, La/Co, and Eu/Eu* indicate felsic source rocks for the sediments. Indeed, sediment supply by Namibian rivers with headwaters originating at the southern Angolan Shield and the Damara Belt should deliver high proportions of felsic, Paleoproterozoic-age rocks (Hawkesworth et al., 1986; McCourt et al., 2013). This implies that

similarly to OGS, there was a shift in source areas from the basal and lower units to the middle unit at OGN where at both sites western source areas became more significant.

Upper and surficial units

Chronostratigraphy

The last phase of sedimentation at the Okavango Basin commenced with the deposition of the sand of the upper units that started not before 1.5 Ma (Figure 3, Table S3). The two dated samples of the upper unit at OGS yielded burial ages of 1.47 +0.14/-0.14 and 1.34 +0.16/−0.14 Ma, while at OGN, two dated samples yielded burial ages between 1.2 +0.14/−0.13 and 1.12 +0.13/−0.12 Ma. These ages imply an early Pleistocene age for the onset of a basin-scale aeolian activity in the Kalahari (Vainer, Dor, et al., 2018). Although the surficial units are not dated in this work because migrating sand (on a multimillennial time-scale) accumulates high concentrations of inherited TCN such that its $^{26}Al/^{10}Be$ ratio exemplifies a complicated burial-exposure history during transport rather a real burial age (Klein et al., 1986; Vainer, Dor, et al., 2018), time constraints can be made for the dynamics of the surficial units. First, the nearly identical TCN concentrations of the surficial and upper units (Table S3) probably imply that exhumation of the surficial sand from its sources occurred not much later than the sand below (comprising the lower units) was deposited. Second, TCN concentrations of the surficial units are an order of magnitude less than concentrations in the southern Kalahari dune field that is migrating for at least 1.5 Myr (Matmon et al., 2015; Matmon, Ron, Chazan, Porat, & Horwitz, 2012; Vainer, Dor, et al., 2018), probably due to shorter residence time for the Kalahari Sand in the Okavango Basin than in the southern Kalahari.

Sediment sources

The similarity in the PSD of the upper and surficial units with PSD of recent aeolian deposits (Thomas et al., 2003, Table S1) suggests that these units were transported and deposited by aeolian processes and that they are composed of mixed sources (McFarlane et al., 2005; Moore & Dingle, 1998). Assuming, at least partly, common sources with the fluvial units below (i.e., the middle units; McFarlane & Eckardt, 2007; Thomas & Shaw, 1991), we refer below to the origins of the fluvial sand in the Okavango Basin to point on some of the sources of the upper and surficial units.

This work confirms that northern Namibia and southern Angola were source areas for the studied sediments, as suggested by bulk geochemical analyses of buried sediments in the Okavango Basin (Huntsman-Mapila et al., 2005). Moreover, we propose that the transition in the proportion of the contribution from sources located to the southeast, east, and northeast in early sedimentation of the basal and lower units to more western and north-western source areas of the middle units (Figure 9), that corroborates with provenance study based on U-Pb ages in zircons of modern river sands that imply on similar changes (Gartner et al., 2014), occurred between ca. 3 and 2 Ma.

Constraints on landscape evolution

The new source areas that became prominent due to the adjustments of the fluvial systems to continental flexure (Cotterill & De Wit, 2011; Moore, 1999) imply on uparching of the western and northwestern flanks of the Okavango Basin (i.e. the Otavi-Caprivi-Mweru and BaKalahari-Schwelle axes), and possibly of the northern Kalahari margins (Lucapa axis; Figure 9). Such a deformation should have resulted in exposure and erosion of the Karoo basalts, that were probably covered until then by Cretaceous sediments (Haddon, 2005). Indeed, although Karoo basalts are not distinctively reflected in the Nd versus Sr isotopic signature of the studied sediments (Figure 7), the Rb-Sr errorchron of the middle and upper units at OGN (Figure 8) suggests a contribution of Karoo-age components following an uplift on basin's periphery.

Deformed features are observed elsewhere in the Okavango and Kalahari basins, exemplifying the effect caused by crustal bending on the depositional environments in these low-relief settings (Figure 1a). Uplift along the Kalahari-Zimbabwe axis and the southern flank of the Chobe Fault that bound the MOZB to the southeast and northeast, respectively (Figures 1b and 9), caused the diversion of river-channels and blocking of southward oriented courses into the evolving endorheic basin (Moore & Larkin, 2001). Amplified by basin's subtle topography, this resulted in the formation of Paleolake Deception that existed more to the east and south of our studied sites, with a minimum formation age of 1.8 Ma (Figure 9, McFarlane & Eckardt, 2006). Subsequent tectonically induced fluvial courses adaptations resulted in the contraction of Paleolake Deception into the >2 times smaller Paleolake Makgadikgadi (Moore et al., 2012). Later activation of faults in the Okavango Basin caused upthrow along the Ghanzi Ridge and Khomas axis (Figure 9) and lead to the ponding of southward oriented rivers, forming the Okavango Delta (McCarthy, 2013; Moore et al., 2012). On the rim of the Kalahari, uplift along the Etosha–Griqualand–Transvaal axis resulted in changes of drainage character and establishment of new waterbodies (Figure 9; Moore, 1999; Stuart-Williams, 1992). Uplift during the Miocene formed Paleolake Etosha (Miller, Pickford, & Senut, 2010) and another episodic bending in the southern Kalahari during the Pleistocene formed the Nossob-Molopo waterbody (Matmon et al., 2015; Vainer, Erel, et al., 2018). The orographic changes that occurred across southern Africa affected regional climate and were coupled with global-scale climatic changes, leading collectively to the supply and distribution of sand to form the vast Kalahari Erg over the desiccated waterbodies (Partridge, 1993, 1998).

The parallel orientation of major faults and the bordering structural axes of the MOZB suggests a link to common tectonic process for which the responsible geodynamical mechanisms are still under debate (Cotterill & De Wit, 2011; Fadel, van der Meijde, & Paulssen, 2018; Haddon & McCarthy, 2005; Moore, 1999; Pastier et al., 2017; Yu et al., 2017). A comprehensive understanding of the triggers that control Okavango Basin's evolution has been hampered by the unique

characteristics of the basin that include: (a) Geomorphological and geological analogies with the EARS where they both have developed over Neoproterozoic suture zones of pre-existing lithospheric weaknesses and lie above thinned crust and lithosphere relative to the thicker bordering terranes (Figures 1 and 2; Chorowicz, 2005; Fadel et al., 2018; Leseane et al., 2015; Yu et al., 2015, 2017). The EARS itself is composed of a unique succession of graben basins linked by intracontinental transforms for which the mechanism of formation is still a subject of discussion (Chorowicz, 2005). (b) The Okavango Basin is superimposed on the vast intracratonic Kalahari Basin where episodic epeirogenic movements have controlled drainage and deposition history (Haddon & McCarthy, 2005; Moore, 1999; Partridge & Maud, 1987). Unambiguous explanations for epeirogenic uplift and downwarp have not been accommodated as these processes probably do not have universal reasoning (Burke & Gunnell, 2008). Further investigation of the propagation of the EARS into southern Africa could lessen the gap of knowledge regarding the driving mechanisms for rifting and epeiorogeny and their possible mantle-driven relations (Burke & Gunnell, 2008; Hansen, Nyblade, & Benoit, 2012).

While the triggers for crustal deformations are beyond the scope of this work, the established spatiotemporal drainage reconstruction provides a time frame for the activity of a major land-forming event that was possibly affected by the southwestward propagation of the EARS. Previous studies were able to characterize the continental geomorphic and sedimentary responses to vertical crustal movements (Holbrook & Schumm, 1999), but age-constrains for these events are usually depended on the presence of deformation- related volcanics, dating erosional forms, or thermal history modelling (De Wit, 2007; Moore, 1999; Quigley, Sandiford, Fifield, & Alimanovic, 2007; Richards, Hoggard, & White, 2016; Sahagian, 1988). The combination of provenance and chronological methods in this work demonstrates a quantitative approach to construct a time frame for the geomorphological response to topographical change.

CONCLUSIONS

We combined 26Al/10Be burial dating with PSD and mineralogy to establish a chronological and litho-stratigraphical framework for Kalahari Group deposition in the western Okavango Basin. The sedimentary sequences that consist of 90 m at the downthrown block south to the Gumare Fault and 36 m thickness at the northern upthrown block started to accumulate at least since the late Pliocene. The first depositional phase of the basal and the lower stratigraphical units ended at both sites around the end of the Pliocene. Provenance analyses based on Pb, Sr and Nd isotopes combined with geochemical proxies reveal that the sediments of these units at the southern block were derived mainly from Proterozoic granitic rocks of the Choma-Koloma Block and the Ghanzi-Chobe and Damara Belts, while some early contribution to a lesser extent from mafic components of the Lufilian Belt

and/or Karoo Basalts is feasible. At the same time period, the northern block received sediments of mostly mafic composition from the Archean, Zimbabwe and Kasai cratons.

The sedimentation on both sides of the Gumare Fault continued at ca. 2 Ma, depositing the middle chrono-stratigraphical units, while source areas of the sediments changed. Following this change, erosional products of felsic composition originating from the Angolan Shield became the main sedimentological component at both sites, possibly supplemented by minor input of weathered Karoo basalts. At the southern block, some mafic input from Archean rocks of the Kasai Craton is also inferred, while the northern block could have also received detritus from the Damara Belt.

The timing of provenance change at both sites coincides with other evidence for rearrangement of the drainage systems that were linked to epeirogenic movements and could be related to the southwestward propagation of the EARS. Early Pleistocene marginal axial uplift and subsidence of the endorheic MOZB substantially altered the landscape and habitable environments of the low-relief landscape. These crustal deformations resulted in the accumulation of large waterbodies within the current semi-arid environment, that were later covered by the aeolian distribution of the far-reaching Kalahari Sand deposits.

Acknowledgements

REFERENCES

- Allen, P. A., & Allen, J. R. (2013). Basin analysis: Principles and application to petroleum play assessment. John Wiley & Sons. T. A. Baillieul (1979). Makgadikgadi pans complex of central Botswana. *Geological Society of America Bulletin*, **90**(2), 289– 312.

- Allen, P. A., & Armitage, J. J. (2011). *Cratonic basins* (pp. 602– 620). Tectonics of sedimentary basins: Recent advances.

- Balco, G. (2017). Production rate calculations for cosmic-ray-muon-produced 10Be and 26Al benchmarked against geological calibration data. *Quaternary Geochronology*, **39**, 150– 173. https://doi.org/10.1016/j.quageo.2017.02.001

- Baldock, J. W., & Evans, J. A. (1988). Constraints on the age of the Bulawayan Group metavolcanic sequence, Harare greenstone belt, Zimbabwe. *Journal of African Earth Sciences (and the Middle East)*, **7**(5–6), 795– 804. https://doi.org/10.1016/0899-5362(88)90022-X

- Bataille, C. P., Laffoon, J., & Bowen, G. J. (2012). Mapping multiple source effects on the strontium isotopic signatures of ecosystems from the circum-Caribbean region. *Ecosphere*, **3**(12), 1– 24. https://doi.org/10.1890/ES12-00155.1

- Bea, F. (2015). Geochemistry of the Lanthanide Elements. XXXV Reunión de la Sociedad Española de Mineralogía.

- Black, L. P., & Shaw, R. D. (1995). An assessment, based on U/Pb zircon data, of Rb/Sr dating in the Arunta Inlier, central Australia. *Precambrian Research*, **71**(1–4), 3– 15.

- Brandt, S., Will, T. M., & Klemd, R. (2007). Magmatic loading in the proterozoic Epupa Complex, NW Namibia, as evidenced by ultrahigh-temperature sapphirine-bearing orthopyroxene–sillimanite–quartz granulites. *Precambrian Research*, **153**(3– 4), 143– 178. https://doi.org/10.1016/j.precamres.2006.11.016

- Braun, J. J., Pagel, M., Muller, J. P., Bilong, P., Michard, A., & Guillet, B. (1990). Cerium anomalies in lateritic profiles. *Geochimica Et Cosmochimica Acta*, **54**(3), 781– 795. https://doi.org/10.1016/0016-7037(90)90373-S

- Brook, S. G., Shaw, G., Bateman, P., Haberyan, M., Appleton, C., … Davies, F. (2003). Late Pleistocene wetting and drying in the NW Kalahari: An integrated study from the Tsodilo Hills, Botswana. *Quaternary International*, **104**, 53– 67. https://doi.org/10.1016/S1040-6182(02)00135-0

- Brown, E. T., Colin, F., & Bourlès, D. L. (2003). Quantitative evaluation of soil processes using in situ-produced cosmogenic nuclides. *Comptes Rendus Geoscience*, **335**(16), 1161– 1171. https://doi.org/10.1016/j.crte.2003.10.004

- Bufford, K. M., Atekwana, E. A., Abdelsalam, M. G., Shemang, E., Atekwana, E. A., Mickus, K., … Molwalefhe, L. (2012). Geometry and faults tectonic activity of the Okavango Rift Zone, Botswana: Evidence from magnetotelluric and electrical resistivity tomography imaging. *Journal of African Earth Sciences*, **65**, 61– 71. https://doi.org/10.1016/j.jafrearsci.2012.01.004

- Burke, K., & Gunnell, Y. (2008). The African erosion surface: a continental-scale synthesis of geomorphology, tectonics, and environmental change over the past 180 million years. *Geological Society of America Memoir* (Vol. **201**, pp. 1– 66). Boulder, Colorado: Geological Society of America. https://doi.org/10.1130/2008.1201

- Burrough, S. L., Thomas, D. S. G., & Bailey, R. M. (2009). Mega-Lake in the Kalahari: A Late Pleistocene record of the Palaeolake Makgadikgadi system. *Quaternary Science Reviews*, **28**(15–16), 1392– 1411. https://doi.org/10.1016/j.quascirev.2009.02.007

- Campbell, G., Johnson, S., Bakaya, T., Kumar, H., & Nsatsi, J. (2006). Airborne geophysical mapping of aquifer water quality and structural controls in the Lower Okavango Delta,

Botswana. *South African Journal of Geology*, **109**(4), 475– 494. https://doi.org/10.2113/gssajg.109.4.475

- Catuneanu, O., Wopfner, H., Eriksson, P. G., Cairncross, B., Rubidge, B. S., Smith, R. M. H., & Hancox, P. J. (2005). The Karoo basins of south-central Africa. *Journal of African Earth Sciences*, **43**(1–3), 211– 253. https://doi.org/10.1016/j.jafrearsci.2005.07.007

- Chorowicz, J. (2005). The east African rift system. *Journal of African Earth Sciences*, **43**(1–3), 379– 410. https://doi.org/10.1016/j.jafrearsci.2005.07.019

- Cockburn, H. A. P., Brown, R. W., Summerfield, M. A., & Seidl, M. A. (2000). Quantifying passive margin denudation and landscape development using a combined fission-track thermochronology and cosmogenic isotope analysis approach. *Earth and Planetary Science Letters*, **179**(3–4), 429– 435. https://doi.org/10.1016/S0012-821X(00)00144-8

- Condie, K. C. (1993). Chemical composition and evolution of the upper continental crust: Contrasting results from surface samples and shales. *Chemical Geology*, **104**(1–4), 1– 37. https://doi.org/10.1016/0009-2541(93)90140-E

- Cooke, H. (1975). The palaeoclimatic significance of caves and adjacent landforms in western Ngamiland. *Botswana. Geographical Journal*, 430– 444. https://doi.org/10.2307/1796477

- Cooke, H. J. (1980). Landform evolution in the context of climatic change and neo-tectonism in the middle Kalahari of northern central Botswana. *Transactions of the Institute of British Geographers*, **5**, 80– 99.

- Cordova, C. E., Scott, L., Chase, B. M., & Chevalier, M. (2017). Late Pleistocene-Holocene vegetation and climate change in the Middle Kalahari, Lake Ngami, Botswana. *Quaternary Science Reviews*, **171**, 199– 215. https://doi.org/10.1016/j.quascirev.2017.06.036

- Cotterill, F. P. D., & De Wit, M. J. (2011). Geoecodynamics and the Kalahari epeirogeny: Linking its genomic record, tree of life and palimpsest into a unified narrative of landscape evolution. *South African Journal of Geology*, **114**(3–4), 489– 514. https://doi.org/10.2113/gssajg.114.3-4.489

- Cullers, R. L. (2000). The geochemistry of shales, siltstones and sandstones of Pennsylvanian-Permian age, Colorado, USA: Implications for provenance and metamorphic studies. *Lithos*, **51**(3), 181– 203. https://doi.org/10.1016/S0024-4937(99)00063-8

- Daly, M. C., Tozer, B., & Watts, A. B. (2019). Cratonic basins and the Wilson cycle: A perspective from the Parnaíba Basin, Brazil. *Geological Society, London, Special Publications*, **470**(1), 463– 477. https://doi.org/10.1144/SP470.13

- Day, J. J., Bills, R., & Friel, J. P. (2009). Lacustrine radiations in African Synodontis catfish. *Journal of Evolutionary Biology*, **22**(4), 805– 817.

- De Carvalho, H., Tassinari, C., Alves, P. H., Guimarães, F., & Simões, M. C. (2000). Geochronological review of the Precambrian in western Angola: Links with Brazil. *Journal of African Earth Sciences*, **31**(2), 383– 402. https://doi.org/10.1016/S0899-5362(00)00095-6

- De Waele, B., Mapani, B. (2002). Geology and correlation of the central Irumide belt. *Journal of African Earth Sciences*, **35**, (3), 385– 397. https://doi.org/10.1016/s0899-5362(02)00149-5

- De Wit, M. (2007). The Kalahari Epeirogeny and climate change: Differentiating cause and effect from core to space. *South African Journal of Geology*, **110**(2–3), 367– 392. https://doi.org/10.2113/gssajg.110.2-3.367

- Delhal, J., Deutsch, S., & Denoiseux, B. (1986). A Sm/Nd isotopic study of heterogeneous granulites from the Archean Kasai-Lomami gabbro-norite and charnockite complex (Zaire, Africa). *Chemical Geology*, **57**(1–2), 235– 245.

- Delhal, J., Ledent, D., & Torquato, J. R. (1977). New geochronological data relating to the gabbro-noritic and charnockitic complex of the Kasai shield and its extension in Angola. *Annals of the Geological Society of Belgium*, **99**, 211– 226. https://popups.uliege.be/0037-9395/index.php?id=5361

- Derricourt, R. M. (1976). Retrogression rate of the Victoria Falls and the Batoka Gorge. *Nature*, **264**(5581), 23– 25.

- Dirks, P. H., & Jelsma, H. A. (2002). Crust–mantle decoupling and the growth of the Archaean Zimbabwe craton. *Journal of African Earth Sciences*, **34**(3–4), 157– 166. https://doi.org/10.1016/S0899-5362(02)00015-5

- Dixey, F. H. (1956). The East African Rift System. *Colonial Geol. Mineral Resources*, **1**, 1– 71.

- Doucouré, C. M., & de Wit, M. J. (2003). Old inherited origin for the present near-bimodal topography of Africa. *Journal of African Earth Sciences*, **36**(4), 371– 388. https://doi.org/10.1016/S0899-5362(03)00019-8

- du Toit, A. L. (1933). Crustal movement as a factor in the geographical evolution of southern Africa. *South African Geographical Journal*, **16**, 3– 20.

- Duncan, R. A., Hooper, P. R., Rehacek, J., Marsh, J., & Duncan, A. R. (1997). The timing and duration of the Karoo igneous event, southern Gondwana. *Journal of Geophysical Research: Solid Earth*, **102**(B8), 18127– 18138. https://doi.org/10.1029/97JB00972

- Ebert, J., & Hitchcock, R. K. (1978). Ancient Lake Makgadikgadi, Botswana: Mapping, measurement and palaeoclimatic significance. *Palaeoecology of Africa*, **10**(11–47), 47– 56.

- Ebinger, C. J. (1989). Tectonic development of the western branch of the East African rift system. *Geological Society of America Bulletin*, **101**(7), 885– 903. https://doi.org/10.1130/0016-7606(1989)101<0885:TDOTWB>2.3.CO;2

- Eckardt, F. E., Flügel, T., Cotterill, F., Rowe, C., & McFarlane, M. (2016). Kalahari tectonic landforms and processes beyond the Okavango Graben. *Quaternary International*, **404**, 194. https://doi.org/10.1016/j.quaint.2015.08.157

- Erel, Y., Dayan, U., Rabi, R., Rudich, Y., & Stein, M. (2006). Trans boundary transport of pollutants by atmospheric mineral dust. *Environmental Science & Technology*, **40**(9), 2996– 3005. https://doi.org/10.1021/es051502l

- Fadel, I., van der Meijde, M., & Paulssen, H. (2018). Crustal structure and dynamics of Botswana. *Journal of Geophysical Research: Solid Earth*, **123**(12), 10– 659. https://doi.org/10.1029/2018JB016190

- Fairhead, J. D., & Girdler, R. W. (1969). How far does the rift system extend through Africa? *Nature*, **221**(5185), 1018– 1020.

- Farmer, G. L., Barber, D., & Andrews, J. (2003). Provenance of Late Quaternary ice-proximal sediments in the North Atlantic: Nd, Sr and Pb isotopic evidence. *Earth and Planetary Science Letters*, **209**(1–2), 227– 243. https://doi.org/10.1016/S0012-821X(03)00068-2

- Faure, G. (1997). *Principles and applications of geochemistry*, Vol. **625**. New Jersey: Prentice Hall.

- Fitzpatrick, R. W., & Chittleborough, D. J. (2002). Titanium and zirconium minerals. *Soil Mineralogy with Environmental Applications*, **7**, 667– 690.

- Garçon, M., Chauvel, C., France-Lanord, C., Limonta, M., & Garzanti, E. (2014). Which minerals control the Nd–Hf–Sr–Pb isotopic compositions of river sediments? *Chemical Geology*, **364**, 42– 55. https://doi.org/10.1016/j.chemgeo.2013.11.018

- Gärtner, A., Linnemann, U., & Hofmann, M. (2014). The provenance of northern Kalahari Basin sediments and growth history of the southern Congo Craton reconstructed by U-Pb ages of zircons from recent river sands. *International Journal of Earth Sciences*, **103**(2), 579– 595. https://doi.org/10.1007/s00531-013-0974-5

- Garzanti, E., Padoan, M., Setti, M., López-Galindo, A., & Villa, I. M. (2014). Provenance versus weathering control on the composition of tropical river mud (southern Africa). *Chemical Geology*, **366**, 61– 74. https://doi.org/10.1016/j.chemgeo.2013.12.016

- Glynn, S. M., Master, S., Wiedenbeck, M., Davis, D. W., Kramers, J. D., Belyanin, G. A., … Oberthür, T. (2017). The Proterozoic Choma-Kalomo Block, SE Zambia: Exotic terrane or a reworked segment of the Zimbabwe Craton? *Precambrian Research*, **298**, 421– 438. https://doi.org/10.1016/j.precamres.2017.06.020

- Goudie, A. S. (2005). The drainage of Africa since the Cretaceous. *Geomorphology*, **67**(3– 4), 437– 456. https://doi.org/10.1016/j.geomorph.2004.11.008

- Government of Botswana (GoB) (2003a): North-western Ngamiland TGLP Groundwater Potential Survey. – Final Report. Department of Geological Surveys, Ministry of Minerals, Energy and Water Affairs.

- Government of Botswana (GoB) (2003b): Geomorphology. Vol. 9. North-western Ngamiland TGLP Groundwater Potential Survey – Final Report. Department of Geological Surveys, Ministry of Minerals, Energy and Water Affairs.

- Granger, D. E., & Muzikar, P. F. (2001). Dating sediment burial with in situ-produced cosmogenic nuclides: Theory, techniques, and limitations. *Earth and Planetary Science Letters*, **188**(1–2), 269– 281. https://doi.org/10.1016/S0012-821X(01)00309-0

- Gray, D. R., Foster, D. A., Meert, J. G., Goscombe, B. D., Armstrong, R., Trouw, R. A. J., & Passchier, C. W. (2008). A Damara orogen perspective on the assembly of southwestern Gondwana. *Geological Society, London, Special Publications*, **294**(1), 257– 278. https://doi.org/10.1144/SP294.14

- Greenwood, P. G., & Carruthers, R. M. (1973). Geophysical surveys in the Okavango Delta. AppliedGeophysics Unit, Institute of Geological Sciences, Report No. 15, 36.

- Grey, D. R. C., & Cooke, H. J. (1977). Some problems in the Quarternary evolution of the landforms of northern Botswana. *Catena*, **4**, 123– 133.

- Grove, A. T. (1969). Landforms and Climatic Change in the Kalahari and Ngamiland. *The Geographical Journal*, **135**(2), 191– 212. https://doi.org/10.2307/1796824

- Gumbricht, T., McCarthy, T. S., & Merry, C. L. (2001). The topography of the Okavango Delta, Botswana, and its tectonic and sedimentological implications. *South African Journal of Geology*, **104**, 243– 264. https://doi.org/10.2113/1040243

- Haddon, I. G. (2005). The Sub-Kalahari Geology and Tectonic Evolution of the Kalahari Basin, Southern Africa. (PhD Thesis, Faculty of Science, University of the Witwatersrand, Johannesburg).

- Haddon, I. G., & McCarthy, T. S. (2005). The Mesozoic-Cenozoic interior sag basins of Central Africa: The late-cretaceous–Cenozoic Kalahari and Okavango Basins. *Journal of African Earth Sciences*, **43**(1–3), 316– 333. https://doi.org/10.1016/j.jafrearsci.2005.07.008

- Haley, B. A., Klinkhammer, G. P., & McManus, J. (2004). Rare earth elements in pore waters of marine sediments. *Geochimica Et Cosmochimica Acta*, **68**(6), 1265– 1279. https://doi.org/10.1016/j.gca.2003.09.012

- Hansen, S. E., Nyblade, A. A., & Benoit, M. H. (2012). Mantle structure beneath Africa and Arabia from adaptively parameterized P-wave tomography: Implications for the origin of Cenozoic Afro-Arabian tectonism. *Earth and Planetary Science Letters*, **319**, 23– 34. https://doi.org/10.1016/j.epsl.2011.12.023

- Hanson, R. E. (2003). Proterozoic geochronology and tectonic evolution of southern Africa. *Geological Society, London, Special Publications*, **206**(1), 427– 463. https://doi.org/10.1144/GSL.SP.2003.206.01.20

- Haughton, P. D. W., Todd, S. P., & Morton, A. C. (1991). Sedimentary provenance studies. *Geological Society, London, Special Publications*, **57**(1), 1– 11. https://doi.org/10.1144/GSL.SP.1991.057.01.01

- Hawkesworth, C. J., Menzies, M. A., & Van Calsteren, P. (1986). Geochemical and tectonic evolution of the Damara Belt, Namibia. *Geological Society, London, Special Publications*, **19**(1), 305– 319. https://doi.org/10.1144/GSL.SP.1986.019.01.17

- Heine, C., Dietmar Müller, R., Steinberger, B., & Torsvik, T. H. (2008). Subsidence in intracontinental basins due to dynamic topography. *Physics of the Earth and Planetary Interiors*, **171**(1), 252– 264. https://doi.org/10.1016/j.pepi.2008.05.008

- Hidy, A. J., Gosse, J. C., Froese, D. G., Bond, J. D., & Rood, D. H. (2013). A latest Pliocene age for the earliest and most extensive Cordilleran Ice Sheet in northwestern Canada. *Quaternary Science Reviews*, **61**, 77– 84. https://doi.org/10.1016/j.quascirev.2012.11.009

- Holbrook, J., & Schumm, S. A. (1999). Geomorphic and sedimentary response of rivers to tectonic deformation: A brief review and critique of a tool for recognizing subtle epeirogenic deformation in modern and ancient settings. *Tectonophysics*, **305**(1–3), 287– 306. https://doi.org/10.1016/S0040-1951(99)00011-6

- Huntsman-Mapila, P., Kampunzu, A. B., Vink, B., & Ringrose, S. (2005). Cryptic indicators of provenance from the geochemistry of the Okavango Delta sediments. *Botswana. Sedimentary Geology*, **174**(1–2), 123– 148. https://doi.org/10.1016/j.sedgeo.2004.11.001

- Huntsman-Mapila, P., Tiercelin, J. J., Benoit, M., Ringrose, S., Diskin, S., Cotten, J., & Hémond, C. (2009). Sediment geochemistry and tectonic setting: Application of discrimination diagrams to early stages of intracontinental rift evolution, with examples from the Okavango and Southern Tanganyika rift basins. *Journal of African Earth Sciences*, **53**(1–2), 33– 44. https://doi.org/10.1016/j.jafrearsci.2008.07.005

- Hutchins, D. G., Hutton, L. G., Hutton, S. M., Jones, C. R., & Loenhert, E. P. (1976). *A Summary of the Geology, Seismicity, Geomorphology and Hydrogeology of the Okavango Delta'*, 7, 1-27. Lobatse, Botswana: Republic of Botswana Geological Survey Department.

- Jacobsen, S. B., & Wasserburg, G. J. (1980). Sm-Nd isotopic evolution of chondrites. *Earth and Planetary Science Letters*, **50**(1), 139– 155. https://doi.org/10.1016/0012-821X(80)90125-9

- Jahn, B. M., & Condie, K. C. (1976). On the age of Rhodesian greenstone belts. *Contributions to Mineralogy and Petrology*, **57**(3), 317– 330. https://doi.org/10.1007/BF03542941

- Jelsma, H. A., McCourt, S., Perritt, S. H., & Armstrong, R. A. (2018). The geology and evolution of the Angolan shield, Congo craton. *Geology of Southwest Gondwana* (pp. 217– 239). Cham: Springer.

- Jelsma, H. A., Perritt, S. H., Armstrong, R. A., & Ferreira, H. F. (2011). SHRIMP U-Pb zircon geochronology of basement rocks of the Angolan Shield, western Angola. Abstract, 23rd CAG, Johannesburg, 8th–14th January.

- Jelsma, H. A., Perritt, S. H., Joy, S., & Armstrong, R. A. (2016). Basement architecture of the Central African Kasai Craton revealed using high precision SHRIMP II U-Pb zircon geochronology. In International Geological Congress (Paper Number: 1835). Cape Town.

- Jelsma, H. A., Vinyu, M. L., Wijbrans, J. R., Verdurmen, E. A. T., Valbracht, P. J., & Davies, G. R. (1996). Constraints on Archaean crustal evolution of the Zimbabwe craton: A U-Pb zircon, Sm-Nd and Pb-Pb whole-rock isotope study. *Contributions to Mineralogy and Petrology*, **124**(1), 55– 70. https://doi.org/10.1007/s004100050173

- Jourdan, F., Bertrand, H., Schärer, U., Blichert-Toft, J., Féraud, G., & Kampunzu, A. B. (2007). Major and trace element and Sr, Nd, Hf, and Pb isotope compositions of the Karoo large igneous province, Botswana–Zimbabwe: Lithosphere vs mantle plume contribution. *Journal of Petrology*, **48**(6), 1043– 1077. https://doi.org/10.1093/petrology/egm010

- Kampunzu, A. B., Akanyang, P., Mapeo, R. B. M., Modie, B. N., & Wendorff, M. (1998). Geochemistry and tectonic significance of the Mesoproterozoic Kgwebe metavolcanic rocks in northwest Botswana: Implications for the evolution of the Kibaran Namaqua-Natal belt. *Geological Magazine*, **135**(5), 669– 683.

- Kampunzu, A. B., Armstrong, R. A., Modisi, M. P., & Mapeo, R. B. (1999). The Kibaran Belt in Southwest Africa: Ion Microprobe U-Pb Zircon Data and Definition of the Kibaran Ngami Belt in Botswana. *Namibia and Angola, Gondwana Research*, **2**(4), 571– 572. https://doi.org/10.1016/S1342-937X(05)70200-8

- Kampunzu, A. B., Armstrong, R. A., Modisi, M. P., & Mapeo, R. B. M. (2000). Ion microprobe U- Pb ages on detrital zircon grains from the Ghanzi Group: Implications for the identification of a Kibaran-age crust in northwest Botswana. *Journal of African Earth Sciences*, **30**(3), 579– 587. https://doi.org/10.1016/S0899-5362(00)00040-3

- Key, R. M., & Rundle, C. C. (1981). The regional significance of new isotopic ages from Precambrian windows through the'Kalahari Beds' in north-western Botswana. *Transactions of the Geological Society of South Africa*, **84**(1), 51– 66.

- Kinabo, B. D., Hogan, J. P., Atekwana, E. A., Abdelsalam, M. G., & Modisi, M. P. (2008). Fault growth and propagation during incipient continental rifting: Insights from a combined aeromagnetic and Shuttle Radar Topography Mission digital elevation model investigation of the Okavango Rift Zone, northwest Botswana. *Tectonics*, **27**(3), 1– 16. https://doi.org/10.1029/2007TC002154

- King, L. C. (1951). *South African Scenery*, 2nd ed. (p. 243). Edinburgh: Oliver and Boyd.

- King, L. C., & King, L. A. (1959). A reappraisal of the Natal monocline. *South African Geographical Journal*, **41**, 15– 30. https://doi.org/10.1080/03736245.1959.10559341

- Klein, J., Giegengack, R., Middleton, R., Sharma, P., Underwood, J. R., & Weeks, R. A. (1986). Revealing histories of exposure using in situ produced 26 Al and 10 Be in Libyan desert glass. *Radiocarbon*, **28**(2A), 547– 555.

- Kohl, C. P., Nishiizumi, K. (1992). Chemical isolation of quartz for measurement of in-situ - produced cosmogenic nuclides. *Geochimica et Cosmochimica Acta*, **56**, (9), 3583– 3587. https://doi.org/10.1016/0016-7037(92)90401-4

- Koppel, V. H., & Saager, R. (1974). Lead isotope evidence on the detrital origin of Witwatersrand pyrites and its bearing on the provenance of the Witwatersrand gold. *Economic Geology*, **69**(3), 318– 331. https://doi.org/10.2113/gsecongeo.69.3.318

- Lancaster, I. N. (1979). Evidence for a widespread late Pleistocene humid period in the Kalahari. *Nature*, **279**(5709), 145. https://doi.org/10.1038/279145a0

- Le Gall, B., Tshoso, G., Jourdan, F., Féraud, G., Bertrand, H., Tiercelin, J., … Maia, M. (2002). 40Ar/39Ar geochronology and structural data from the giant Okavango and related mafic dyke swarms, Karoo igneous province, northern Botswana. *Earth and Planetary Science Letters*, **202**(3–4), 595– 606. https://doi.org/10.1016/S0012-821X(02)00763-X

- Leighton, M. W., & Kolata, D. R. (1990). Selected Interior Cratonic Basins and Their Place in the Scheme of Global Tectonics: A Synthesis: Chapter 35: Part III. Synthesis and Analysis of Interior Cratonic Basins: Synthesis, (729-797).

- Leseane, K., Atekwana, E. A., Mickus, K. L., Abdelsalam, M. G., Shemang, E. M., & Atekwana, E. A. (2015). Thermal perturbations beneath the incipient Okavango Rift Zone, Northwest Botswana. *Journal of Geophysical Research: Solid Earth*, **120**(2), 1210– 1228. https://doi.org/10.1002/2014JB011029

- Lifton, N., Sato, T., & Dunai, T. J. (2014). Scaling in situ cosmogenic nuclide production rates using analytical approximations to atmospheric cosmic-ray fluxes. *Earth and Planetary Science Letters*, **386**, 149– 160. https://doi.org/10.1016/j.epsl.2013.10.052

- Lister, L. A. (1979). The geomorphic evolution of Zimbabwe Rhodesia. *South African Journal of Geology*, **82**(3), 363– 370.

- Logatchev, N. A., Beloussov, V. V., & Milanovsky, E. E. (1972). East african rift development. In R. W. Girdler (Ed.), East African Rifts. *Tectonophysics*, **15**(1-2), 71– 81. https://doi.org/10.1016/0040-1951(72)90053-4

- Mallick, D. I. J., Habgood, F., & Skinner, A. C. (1981). *Geological interpretation of Landsat imagery and air photography of Botswana*, Overseas Geology and Mineral Resources, **56**, (35– 36). H.M. Stationery Office. Retrieved from https://books.google.co.il/books/about/Geological_Interpretation_of_Landsat_Ima.html?id=FvgeAQAAIAAJ&redir_esc=y

- Mapeo, R. B. M., Armstrong, R. A., & Kampunzu, A. B. (2001). SHRIMP U-Pb zircon geochronology of gneisses from the Gweta borehole, northeast Botswana: Implications for the Palaeoproterozoic Magondi Belt in southern Africa. *Geological Magazine*, **138**(3), 299– 308.

- Mapeo, R. B. M., Kampunzu, A. B., & Armstrong, R. A. (2000). Ages of detrital zircon grains from Neoproterozoic siliciclastic rocks in the Shakawe area: Implications for the evolution of Proterozoic crust in northern Botswana. *South African Journal of Geology*, **103**(2), 156– 161. https://doi.org/10.2113/103.2.156

- Marsh, J. S. (1991). REE fractionation and Ce anomalies in weathered Karoo dolerite. *Chemical Geology*, **90**(3–4), 189– 194. https://doi.org/10.1016/0009-2541(91)90099-D

- Matmon, A., Hidy, A. J., Vainer, S., Crouvi, O., Fink, D., Erel, Y., … Horwitz, L. K. (2015). New chronology for the southern Kalahari Group sediments with implications for sediment-cycle dynamics and early hominin occupation. *Quaternary Research*, **84**(1), 118– 132. https://doi.org/10.1016/j.yqres.2015.04.009

- Matmon, A., Ron, H., Chazan, M., Porat, N., & Horwitz, L. K. (2012). Reconstructing the history of sediment deposition in caves: A case study from Wonderwerk Cave. *South Africa. Bulletin*, **124**(3–4), 611– 625. https://doi.org/10.1130/B30410.1

- McCarthy, T. S. (2013). The Okavango Delta and its place in the geomorphological evolution of southern Africa. *South African Journal of Geology*, **116**(1), 1– 54. https://doi.org/10.2113/gssajg.116.1.1

- McCarthy, T. S., & Ellery, W. N. (1998). The Okavango delta. *Transactions of the Royal Society of South Africa*, **53**(2), 157– 182. https://doi.org/10.1080/00359199809520384

- McCarthy, T. S., Green, R. W., & Franey, N. J. (1993). The influence of neo-tectonics on water dispersal in the northeastern regions of the Okavango swamps, Botswana. *Journal of African Earth Sciences*, **17**(1), 23– 32. https://doi.org/10.1016/0899-5362(93)90019-M

- McCarthy, T. S., McIver, J. R., & Verhagen, B. T. (1991). Groundwater evolution, chemical sedimentation and carbonate brine formation on an island in the Okavango Delta swamp, Botswana. *Applied Geochemistry*, **6**(6), 577– 595. https://doi.org/10.1016/0883-2927(91)90071-V

- McCarthy, T. S., Smith, N. D., Ellery, W. N., & Gumbricht, T. (2002). The Okavango Delta—semiarid alluvial-fan sedimentation related to incipient rifting. *SEPM Special Publication*, **73**, 173– 179.

- McCourt, S., Armstrong, R. A., Jelsma, H., & Mapeo, R. B. M. (2013). New U-Pb SHRIMP ages from the Lubango region, SW Angola: Insights into the Palaeoproterozoic evolution of the Angolan Shield, southern Congo Craton, Africa. *Journal of the Geological Society*, **170**(2), 353– 363. https://doi.org/10.1144/jgs2012-059

- McFarlane, M. J., Coetzee, S. H., Kuhn, J. R., Vanderpost, C. H. M., & Eckardt, F. D. (2007). In situ rounding of quartz grains within an African surface weathering profile in North West Ngamiland. *Botswana. Zeitschrift Für Geomorphologie*, **51**(3), 269– 286. https://doi.org/10.1127/0372-8854/2007/0051-0269

- McFarlane, M. J., & Eckardt, F. D. (2006). Lake Deception: A new Makgadikgadi palaeolake. *Botswana Notes and Records*, **38**, 195– 201.

- McFarlane, M. J., & Eckardt, F. D. (2007). Palaeodune morphology associated with the Gumare fault of the Okavango graben in the Botswana/Namibia borderland: A new model of tectonic influence. *South African Journal of Geology*, **110**(4), 535– 542. https://doi.org/10.2113/gssajg.110.4.535

- McFarlane, M. J., Eckardt, F. D., Ringrose, S., Coetzee, S. H., & Kuhn, J. R. (2005). Degradation of linear dunes in Northwest Ngamiland, Botswana and the implications for luminescence dating of periods of aridity. *Quaternary International*, **135**(1), 83– 90. https://doi.org/10.1016/j.quaint.2004.10.025

- McFarlane, M. J., & Segadika, P. (2001). Archaeological evidence for the reassessment of the ages of the Makgadikgadi paleolakes. *Botswana Notes & Records*, **33**(1), 83– 90.

- McKenzie, D. M., & Priestley, K. (2016). Speculations on the formation of cratons and cratonic basins. *Earth and Planetary Science Letters*, **435**, 94– 104. https://doi.org/10.1016/j.epsl.2015.12.010

- McLennan, S. M., Hemming, S., McDaniel, D. K., & Hanson, G. N. (1993). Geochemical approaches to sedimentation, provenance, and tectonics. *Special Papers-Geological Society of America*, 21.

- Meier, P., Kalscheuer, T., Podgorski, J. E., Kgotlhang, L., Green, A. G., Greenhalgh, S., … Mikkelsen, P. (2014). Hydrogeophysical investigations in the western and north-central Okavango Delta (Botswana) based on helicopter and ground-based transient electromagnetic data and electrical resistance tomography. *Geophysics*, **79**(5), B201– B211. https://doi.org/10.1190/geo2014-0001.1

- Miller, R. M. (2014). Evidence for the evolution of the Kalahari dunes from the Auob River, southeastern Namibia. *Transactions of the Royal Society of South Africa*, **69**(3), 195– 204. https://doi.org/10.1080/0035919X.2014.955555

- Miller, R. M., Pickford, M., & Senut, B. (2010). The geology, palaeontology and evolution of the Etosha Pan, Namibia: Implications for terminal Kalahari deposition. *South African Journal of Geology*, **113**(3), 307– 334. https://doi.org/10.2113/gssajg.113.3.307

- Milner, S. C., Duncan, A. R., Whittingham, A. M., & Ewart, A. (1995). Trans-Atlantic correlation of eruptive sequences and individual silicic volcanic units within the Paraná-Etendeka igneous province. *Journal of Volcanology and Geothermal Research*, **69**(3–4), 137– 157. https://doi.org/10.1016/0377-0273(95)00040-2

- Modie, B. N. (1996). Depositional environments of the Meso-to Neoproterozoic Ghanzi-Chobe belt, northwest Botswana. *Journal of African Earth Sciences*, **22**(3), 255– 268. https://doi.org/10.1016/0899-5362(96)00014-0

- Modisi, M. P. (2000). Fault system at the southeastern boundary of the Okavango Rift, Botswana. *Journal of African Earth Sciences*, **30**(3), 569– 578. https://doi.org/10.1016/S0899-5362(00)00039-7

- Modisi, M. P., Atekwana, E. A., Kampunzu, A. B., & Ngwisanyi, T. H. (2000). Rift kinematics during the incipient stages of continental extension: Evidence from the nascent Okavango rift basin, northwest Botswana. *Geology*, **28**(10), 939– 942.

- Moore, A. E. (1999). A reappraisal of epeirogenic flexure axes in southern Africa. *South African Journal of Geology*, **102**(4), 363– 376.

- Moore, A., Blenkinsop, T., & Cotterill, F. (2009). Southern African topography and erosion history: Plumes or plate tectonics? *Terra Nova*, **21**(4), 310– 315. https://doi.org/10.1111/j.1365-3121.2009.00887.x

- Moore, A. E., Cotterill, F. P. D., & Eckardt, F. D. (2012). The evolution and ages of Makgadikgadi palaeo-lakes: Consilient evidence from Kalahari drainage evolution south-central Africa. *South African Journal of Geology*, **115**(3), 385– 413. https://doi.org/10.2113/gssajg.115.3.385

- Moore, A. E., & Dingle, R. V. (1998). Evidence for fluvial sediment transport of Kalahari sands in central Botswana. *South African Journal of Geology*, **101**(2), 143– 153.

- Moore, A. E., & Larkin, P. A. (2001). Drainage evolution in south-central Africa since the breakup of Gondwana. *South African Journal of Geology*, **104**(1), 47– 68. https://doi.org/10.2113/104.1.47

- Moorkamp, M., Fishwick, S., Walker, R. J., Jones, A. G., & Mt, C. (2019). Geophysical evidence for crustal and mantle weak zones controlling intra-plate seismicity – the 2017 Botswana earthquake sequence. *Earth and Planetary Science Letters*, **506**, 175– 183. https://doi.org/10.1016/j.epsl.2018.10.048

- Napier, T. J., Hendy, I. L., Fahnestock, M. F., & Bryce, J. G. (2020). Provenance of detrital sediments in Santa Barbara Basin, California, USA: Changes in source contributions between the Last Glacial Maximum and Holocene. *GAS Bulletin*, **132**(1–2), 65– 84. https://doi.org/10.1130/B32035.1

- NASA JPL (2013). NASA Shuttle Radar Topography Mission Global 30 arc second. NASA EOSDIS Land Processes DAAC. Retrieved from 10.5067/MEaSUREs/SRTM/SRTMGL30.002

- Nash, D. J., & Eckardt, F. D. (2016). Drainage development, neotectonics and base-level change in the Kalahari Desert, southern Africa. *South African Geographical Journal*, **98**(2), 308– 320. https://doi.org/10.1080/03736245.2015.1028987

- Padoan, M., Garzanti, E., Harlavan, Y., & Villa, I. M. (2011). Tracing nile sediment sources by Sr and Nd isotope signatures (Uganda, Ethiopia, Sudan). *Geochimica Et Cosmochimica Acta*, **75**(12), 3627– 3644. https://doi.org/10.1016/j.gca.2011.03.042

- Palchan, D., Stein, M., Almogi-Labin, A., Erel, Y., & Goldstein, S. L. (2013). Dust transport and synoptic conditions over the Sahara-Arabia deserts during the MIS6/5 and 2/1 transitions from grain-size, chemical and isotopic properties of Red Sea cores. *Earth and Planetary Science Letters*, **382**, 125– 139. https://doi.org/10.1016/j.epsl.2013.09.013

- Partridge, T. C. (1993). The evidence for Cainozoic aridification in southern Africa. *Quaternary International*, **17**, 105– 110. https://doi.org/10.1016/1040-6182(93)90087-V

- Partridge, T. C. (1998). Of diamonds, dinosaurs and diastrophism: 150 million years of landscape evolution in southern Africa. *South African Journal of Geology*, **101**(3), 167– 184.

- Partridge, T. C., & Maud, R. R. (1987). Geomorphic evolution of southern Africa since the Mesozoic. *South African Journal of Geology*, **90**(2), 179– 208.

- Pastier, A., Dauteuil, O., Murray-hudson, M., & Moreau, F. (2017). Tectonophysics Is the Okavango Delta the terminus of the East African Rift System ? Towards a new geodynamic model : Geodetic study and geophysical review. *Tectonophysics*, **712–713**, 469– 481.

- Pattan, J. N., Pearce, N. J. G., & Mislankar, P. G. (2005). Constraints in using Cerium-anomaly of bulk sediments as an indicator of paleo bottom water redox environment: A case study from the Central Indian Ocean Basin. *Chemical Geology*, **221**(3–4), 260– 278. https://doi.org/10.1016/j.chemgeo.2005.06.009

- Podgorski, J. E., Green, A. G., Kgotlhang, L., Kinzelbach, W. K., Kalscheuer, T., Auken, E., & Ngwisanyi, T. (2013). Paleo-megalake and paleo-megafan in southern Africa. *Geology*, **41**(11), 1155– 1158. https://doi.org/10.1130/G34735.1

- Quigley, M., Sandiford, M., Fifield, L. K., & Alimanovic, A. (2007). Landscape responses to intraplate tectonism: Quantitative constraints from 10Be nuclide abundances. *Earth and Planetary Science Letters*, **261**(1–2), 120– 133. https://doi.org/10.1016/j.epsl.2007.06.020

- Rainaud, C., Master, S., Armstrong, R. A., & Robb, L. J. (2005). Geochronology and nature of the Palaeoproterozoic basement in the Central African Copperbelt (Zambia and the Democratic Republic of Congo), with regional implications. *Journal of African Earth Sciences*, **42**(1–5), 1– 31. https://doi.org/10.1016/j.jafrearsci.2005.08.006

- Ramokate, L. V., Mapeo, R. M. M., Corfu, F., & Kampunzu, A. B. (2000). Proterozoic geology and regional correlation of the Ghanzi-Makunda area, western Botswana. *Journal of African Earth Sciences*, **30**(3), 453– 466. https://doi.org/10.1016/S0899-5362(00)00031-2

- Reeves, C. V., & Hutchins, D. G. (1982). A progress report on the geophysical exploration of the Kalahari in Botswana. *Geoexploration*, **20**(3–4), 209– 224. https://doi.org/10.1016/0016-7142(82)90022-9

- Richards, F. D., Hoggard, M. J., & White, N. J. (2016). Cenozoic epeirogeny of the Indian peninsula. *Geochemistry, Geophysics, Geosystems*, **17**(12), 4920– 4954. https://doi.org/10.1002/2016GC006545

- Ringrose, S., Huntsman-Mapila, P., Downey, W., Coetzee, S., Fey, M., Vanderpost, C., … Kolokose, D. (2008). Diagenesis in Okavango fan and adjacent dune deposits with implications for the record of palaeo-environmental change in Makgadikgadi–Okavango–Zambezi basin, northern Botswana. *Geomorphology*, **101**(4), 544– 557. https://doi.org/10.1016/j.geomorph.2008.02.008

- Ringrose, S., Huntsman-Mapila, P., Kampunzu, A. B., Downey, W., Coetzee, S., Vink, B., … Vanderpost, C. (2005). Sedimentological and geochemical evidence for palaeo-environmental change in the Makgadikgadi subbasin, in relation to the MOZ rift depression, Botswana. *Palaeogeography, Palaeoclimatology, Palaeoecology*, **217**(3–4), 265– 287. https://doi.org/10.1016/j.palaeo.2004.11.024

- Rodrigo-Gámiz, M., Martínez-Ruiz, F., Chiaradia, M., Jiménez-Espejo, F. J., & Ariztegui, D. (2015). Radiogenic isotopes for deciphering terrigenous input provenance in the western Mediterranean. *Chemical Geology*, **410**, 237– 250. https://doi.org/10.1016/j.chemgeo.2015.06.004

- Sahagian, D. (1988). EPeirogenic motions of Africa as inferred from Cretaceous shoreline deposits. *Tectonics*, **7**(1), 125– 138. https://doi.org/10.1029/TC007i001p00125

- Schlüter, T., (2008). *Geological atlas of Africa with notes on stratigraphy, tectonics, economic geology, geohazards and geosites of each country*, Springer, Berlin, Heidelberg: Springer Science & Business Media. https://doi.org/10.1007/3-540-29145-8

- Scholz, C. H., Koczynski, T. A., & Hutchins, D. G. (1976). Evidence for incipient rifting in southern Africa. *Geophysical Journal International*, **44**(1), 135– 144. https://doi.org/10.1111/j.1365-246X.1976.tb00278.x

- Shaw, P. A. (1985). Late Quaternary landforms and environmental change in northwest Botswana: The evidence of Lake Ngami and the Mababe Depression. *Transactions Institute of British Geographers*, **NS10**, 333– 346. https://doi.org/10.2307/622182

- Shaw, P. A., & Thomas, D. S. G. (1988). Lake Caprivi, a late Quaternary link between the Zambezi middle Kalahari drainage systems. *Zeitschrift Für Geomorphologie*, **32**, 329– 337.

- Singletary, S. J., Hanson, R. E., Martin, M. W., Crowley, J. L., Bowring, S. A., Key, R. M., … Krol, M. A. (2003). Geochronology of basement rocks in the Kalahari Desert, Botswana, and implications for regional Proterozoic tectonics. *Precambrian Research*, **121**(1–2), 47– 71. https://doi.org/10.1016/S0301-9268(02)00201-2

- Sleep, N. H. (1971). Thermal effects of the formation of Atlantic continental margins by continental break up. *Geophysical Journal of the Royal Astronomical Society*, **24**(4), 325– 350. https://doi.org/10.1111/j.1365-246X.1971.tb02182.x

- Sloss, L. L., & Speed, R. C. (1974). Relationships of cratonic and continental-margin tectonic episodes. *SEPM Special Publication*, **22**, 98– 119.

- Smith, R. A. (1984). The lithostratigraphy of the Karoo Supergroup in Botswana (26). Geological Survey Department with the authority of Ministry of Mineral Resources and Water Affairs, Republic of Botswana.

- Stein, M., Starinsky, A., Katz, A., Goldstein, S. L., Machlus, M., & Schramm, A. (1997). Strontium isotopic, chemical, and sedimentological evidence for the evolution of Lake Lisan and the Dead Sea. *Geochimica Et Cosmochimica Acta*, **61**(18), 3975– 3992. https://doi.org/10.1016/S0016-7037(97)00191-9

- Stuart-Williams, V. (1992). Overall tectonics, modern basin evolution and groundwater chemistry of the Owambo Basin. Abstracts, Kalahari Symposium, Geological Society of Namibia, Windhoek, 3-9.

- Tanaka, T., Togashi, S., Kamioka, H., Amakawa, H., Kagami, H., Hamamoto, T., … Kunimaru, T. (2000). JNdi-1: A neodymium isotopic reference in consistency with LaJolla neodymium. *Chemical Geology*, **168**(3–4), 279– 281. https://doi.org/10.1016/S0009-2541(00)00198-4

- Taylor, S. R., & McLennan, S. M. (1981). The composition and evolution of the continental crust: Rare earth element evidence from sedimentary rocks. *Philosophical Transactions of the Royal Society of London. Series A, Mathematical and Physical Sciences*, **301**(1461), 381– 399.

- Taylor, S. R., & McLennan, S. M. (1985). *The continental crust: Its composition and evolution* (pp. 1– 312). Oxford: Blackwell Scientific Publications.

- Thiéblemont, D., Callec, Y., Fernandez-Alonso, M., & Chène, F. (2018). A geological and isotopic framework of Precambrian terrains in western Central Africa: An introduction. In S. Siegesmund M. A. S. Basei P. Oyhantçabal & S. Oriolo (eds.), *Geology of Southwest Gondwana* (pp. 107– 132). Cham: Springer. https://doi.org/10.1007/978-3-319-68920-3_5

- Thomas, D. S., Brook, G., Shaw, P., Bateman, M., Haberyan, K., Appleton, C., …Davies, F. (2003). Late Pleistocene wetting and drying in the NW Kalahari: An integrated study from the Tsodilo Hills, Botswana. *Quaternary International*, **104**(1), 53– 67. https://doi.org/10.1016/S1040-6182(02)00135-0

- Thomas, D. S., & Shaw, P. A. (1991). *The Kalahari Environment* (pp. 1– 284). Cambridge: Cambridge University Press.

- Vainer, S., Dor, Y. B., & Matmon, A. (2018). Coupling cosmogenic nuclides and luminescence dating into a unified accumulation model of aeolian landforms age and dynamics: The case study of the Kalahari Erg. *Quaternary Geochronology*, **48**, 133– 144. https://doi.org/10.1016/j.quageo.2018.08.002

- Vainer, S., Erel, Y., & Matmon, A. (2018). Provenance and depositional environments of Quaternary sediments in the southern Kalahari Basin. *Chemical Geology*, **476**, 352– 369. https://doi.org/10.1016/j.chemgeo.2017.11.031

- Vermeesch, P. (2018). IsoplotR: A free and open toolbox for geochronology. *Geoscience Frontiers*, **9**(5), 1479– 1493. https://doi.org/10.1016/j.gsf.2018.04.001

- Wendorff, M., & Master, S. (2015). Lithological variations of sedimentary succession within a meteorite impact crater: Jwaneng S Structure, Botswana. *Geology, Geophysics and Environment*, **41**(4), 381.

- Wronkiewicz, D. J., & Condie, K. C. (1987). Geochemistry of Archean shales from the Witwatersrand Supergroup, South Africa: Source-area weathering and

provenance. *Geochimica Et Cosmochimica Acta*, **51**(9), 2401– 2416. https://doi.org/10.1016/0016-7037(87)90293-6

- Yu, Y., Liu, K. H., Huang, Z., Zhao, D., Reed, C. A., Moidaki, M., … Gao, S. S. (2017). Mantle structure beneath the incipient Okavango rift zone in southern Africa. *Geosphere*, **13**(1), 102– 111. https://doi.org/10.1130/GES01331.1

- Yu, Y., Liu, K. H., Reed, C. A., Moidaki, M., Mickus, K., Atekwana, E. A., & Gao, S. S. (2015). A joint receiver function and gravity study of crustal structure beneath the incipient Okavango Rift. *Botswana. Geophysical Research Letters*, **42**(20), 8398– 8405. https://doi.org/10.1002/2015GL065811